Supplementary Information

for

High accuracy measurements of nanometer-scale distances between fluorophores at the single-molecule level

Stefan Niekamp[1], Jongmin Sung[1], Walter Huynh[1], Gira Bhabha[2], Ronald D. Vale[1]*, and Nico Stuurman[1]

[1] Department of Cellular and Molecular Pharmacology and the Howard Hughes Medical Institute, University of California, San Francisco, 600 16th Street, San Francisco, CA 94158.
[2] Skirball Institute of Biomolecular Medicine, New York University School of Medicine, New York, NY 10016

* Corresponding author: ron.vale@ucsf.edu

This document includes:

Supplementary Information Figures (Fig. S1 - S18)
Supplementary Information Tables (Table S1 - S6)
Supplementary Information Notes (1-3)
Supplementary Information Protocol
References for the Supplementary Information

Supplementary Information Figures

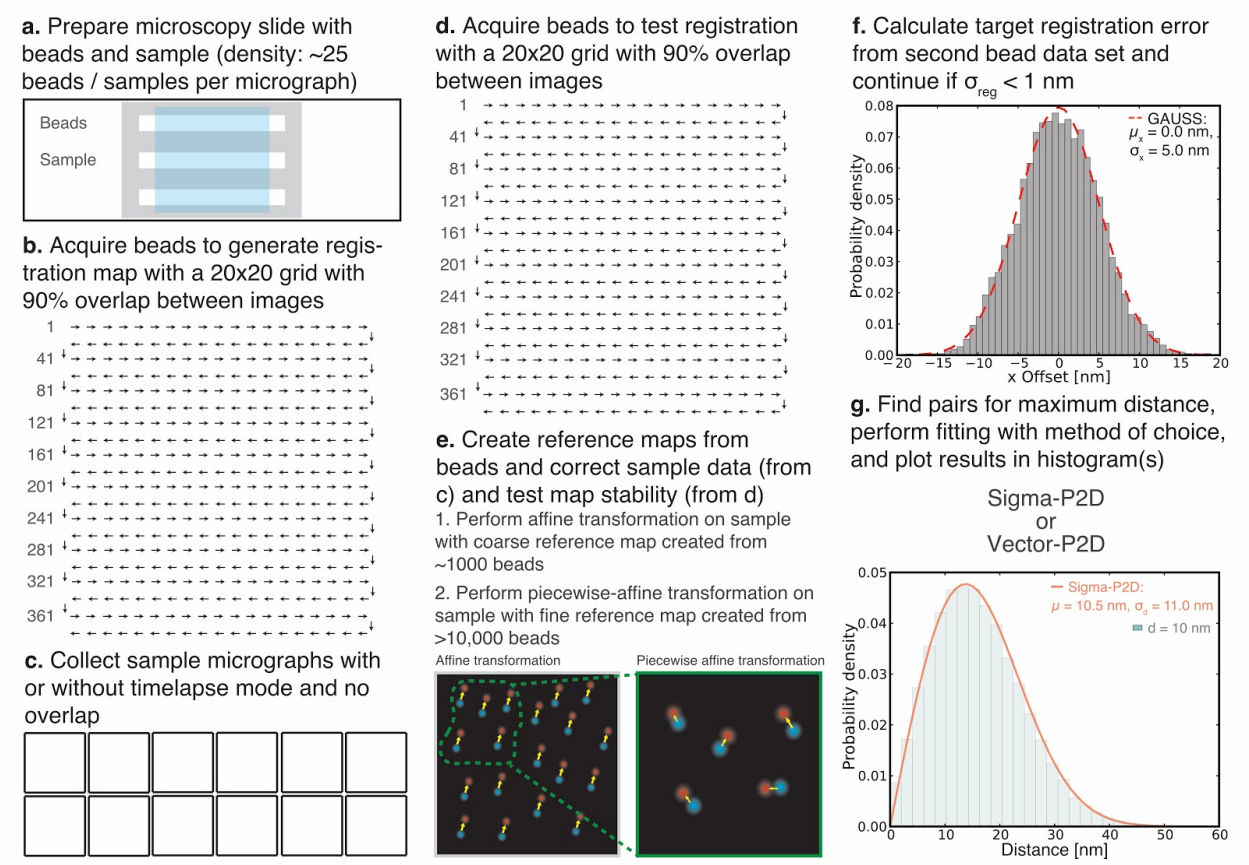

Fig. S1 | Workflow for image registration and distance measurements. (a) Set-up of microscope slide with fiducial markers in one and sample of interest in the another chamber. (b) Image acquisition pattern for fiducial markers to create registration map. (c) Image acquisition pattern for sample of interest. (d) Same as in b but this time to test the registration map after sample data collection. (e) μManager (1) analysis procedure to create affine and piecewise affine registration maps. (f) Calculation of image registration accuracy. (g) μManager (1) analysis procedure to determine distance distribution with Sigma-P2D (sample uniform in distance) or Vector-2D (sample heterogeneous / variable in distance). For more details see SI Protocol.

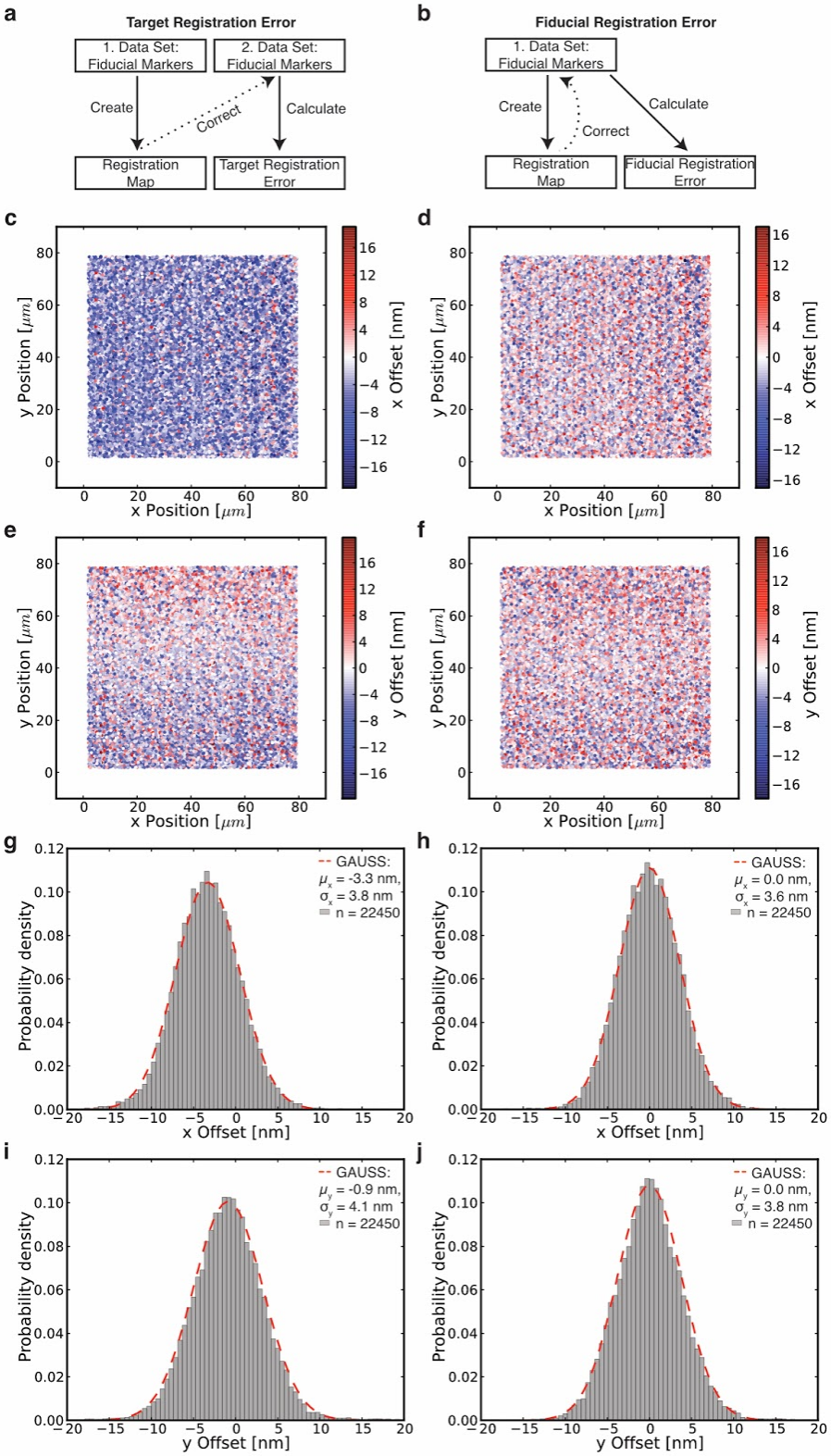
a
Target Registration Error
1. Data Set: Fiducial Markers
2. Data Set: Fiducial Markers
Create
Correct
Calculate
Registration Map
Target Registration Error
b
Fiducial Registration Error
1. Data Set: Fiducial Markers
Create
Correct
Calculate
Registration Map
Fiducial Registration Error
c
d
e
f
y Position [μm]
x Position [μm]
x Offset [nm]
y Offset [nm]
g
h
i
j
Probability density
x Offset [nm]
y Offset [nm]
GAUSS:
μ_x = -3.3 nm,
σ_x = 3.8 nm
n = 22450
μ_x = 0.0 nm,
σ_x = 3.6 nm
μ_y = -0.9 nm,
σ_y = 4.1 nm
μ_y = 0.0 nm,
σ_y = 3.8 nm

Fig. S2 | Comparison of target registration error (TRE) and fiducial registration error (FRE) shows that FRE is unreliable and that TRE should always be reported as registration error. (a) Workflow for target registration error (TRE) calculation. (b) Workflow for fiducial registration error (FRE) calculation. (c-j) The same registration map is used for both, TRE and FRE, but different data sets are used to test the map. For TRE we use an additional fiducial marker data set to evaluated the map while for FRE we use the same data set (fiducial markers) to create and test the registration map. (c) Distance offset along the x-axis for TRE. Each dot shows a single fiducial marker for which the distance offset between the two colors of the same fiducial marker is colorcoded. Negative values (blue dots) mean that channel 1 has a smaller number for its position whereas positive values (red dots) represent fiducials where channel 2 has a smaller number for its position. (d) Same as in c but for FRE. (e) Distance offset between the two colors of the same fiducial marker along the y-axis for TRE. (f) Same as in e but for FRE. (g) Histogram of x-axis offsets with Gaussian fit (dashed red line) for TRE. (h) Same as in g but for FRE. (i) Histogram of y-axis offset with Gaussian fit (dashed red line) for TRE. (j) Same as in i but for FRE. One frame per TetraSpeck™ bead was acquired. Details about fitting parameters in Table S4.

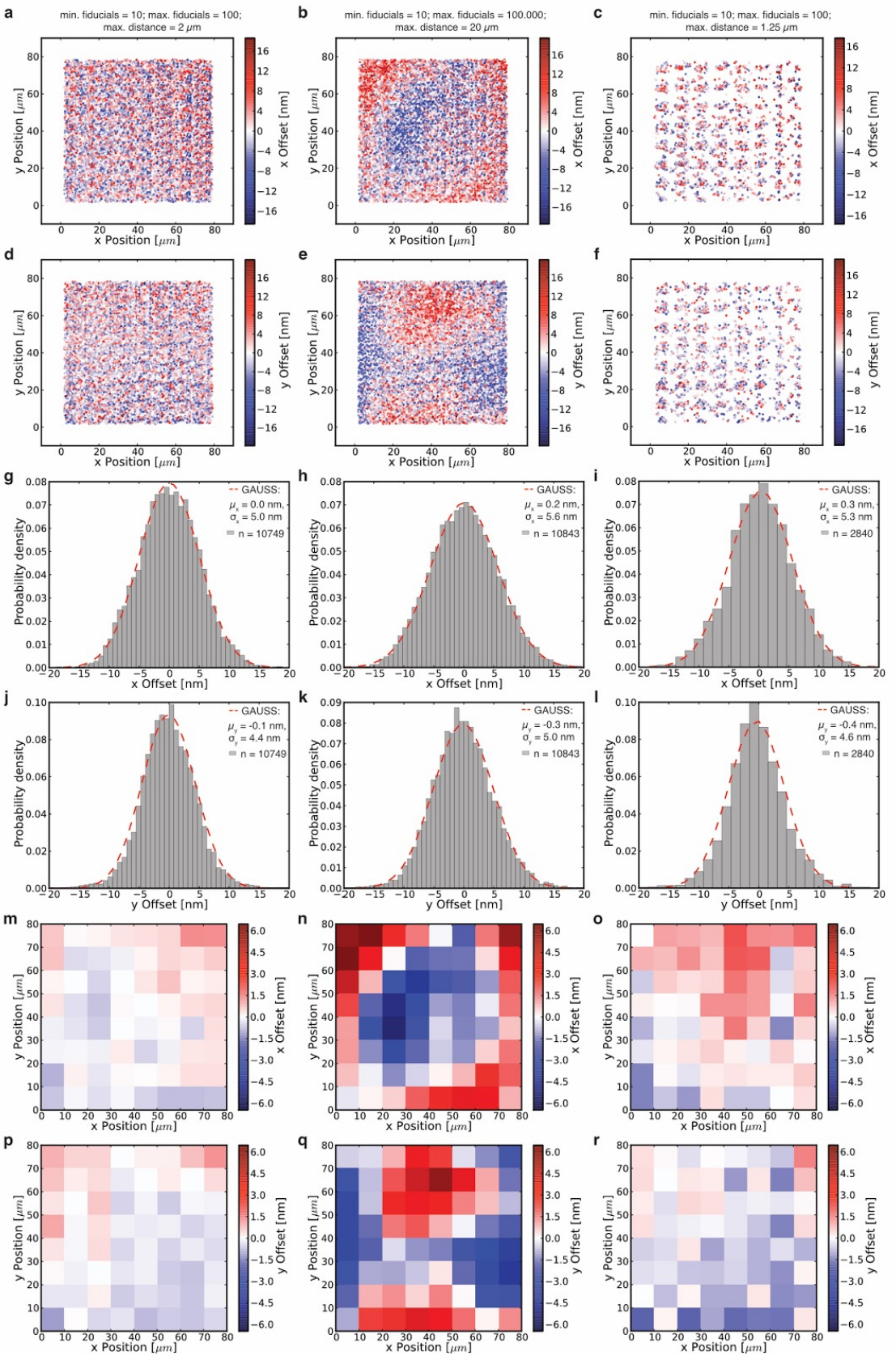
a
min. fiducials = 10; max. fiducials = 100;
max. distance = 2 μm
b
min. fiducials = 10; max. fiducials = 100.000;
max. distance = 20 μm
c
min. fiducials = 10; max. fiducials = 100;
max. distance = 1.25 μm
d
e
f
g
GAUSS:
μx = 0.0 nm,
σx = 5.0 nm
n = 10749
h
GAUSS:
μx = 0.2 nm,
σx = 5.6 nm
n = 10843
i
GAUSS:
μx = 0.3 nm,
σx = 5.3 nm
n = 2840
j
GAUSS:
μy = -0.1 nm,
σy = 4.4 nm
n = 10749
k
GAUSS:
μy = -0.3 nm,
σy = 5.0 nm
n = 10843
l
GAUSS:
μy = -0.4 nm,
σy = 4.6 nm
n = 2840
m
n
o
p
q
r
x Position [μm]
y Position [μm]
x Offset [nm]
y Offset [nm]
Probability density

Fig. S3 | Comparison of different parameters for piecewise affine image registration. TetraSpeck™ beads were imaged, localized and registered using a previously determined registration map with different parameter settings for the piecewise affine transformation. The first parameter setting has a minimum of 10, a maximum of 100 fiducial points and a maximum distance of 2 μm. The second parameter setting has a minimum of 10, maximum of 100,000 fiducial points and maximum distance of 20 μm. The third parameter setting uses a minimum of 10, maximum of 100 fiducial points and maximum distance of 1.25 μm. The data presented in this figure clearly shows that there are significant differences between settings for the piecewise affine correction and that a more detailed analysis is needed (see Fig. S4). (a) Distance offset along the x-axis for first setting. Each dot shows a single fiducial marker for which the distance offset between the two colors of the same fiducial marker is colorcoded. Negative values (blue dots) mean that channel 1 has a smaller number for its x position whereas positive values (red dots) represent fiducials where channel 2 has a smaller number for its x position. (b) Same as in a but for second setting. (c) Same as in a but for third setting. Registration of many beads fails (hence the sparse number of points) because often less than 10 fiducial points are present within 1.25 μm. (d) Distance offset along the y-axis for first setting. Negative values (blue dots) mean that channel 1 has a smaller number for its y position whereas positive values (red dots) represent fiducials where channel 2 has a smaller number for its y position. (e) Same as in d but for second setting. (f) Same as in d but for third setting. (g) Histogram of x-axis offset with Gaussian fit (dashed red line) of data in a. (h) Same as in g but for second setting and of data in b. (i) Same as in g but for third setting and of data in c. (j) Histogram of y-axis offset with Gaussian fit (dashed red line) of data in d. (k) Same as in j but for second setting and of data in e. (l) Same as in j but for third setting and of data in f. (m-r) In order to evaluate the degree of correlation of the registration error between different areas of the micrograph we pooled data in a grid consisting of squares of 10 μm by 10 μm. If for instance the registration error is correlated over the entire field of view or over large areas of the field of view, we expect homogenous coloring in either blue or red among adjacent bins (as in n) whereas for uncorrelated registration errors we expect a random distribution of squares with light shades of red and blue (as in m). (m) Same data as in a but with data binned in 10 μm by 10 μm squares. (n) Same data as in b but with data binned in 10 μm by 10 μm squares. (o) Same data as in c but with data binned in 10 μm by 10 μm squares. (p) Same data as in d but with data binned in 10 μm by 10 μm squares. (q) Same data as in e but with data binned in 10

μm by 10 μm squares. (r) Same data as in f but with data binned in 10 μm by 10 μm squares. Details about fitting parameters in Table S4.

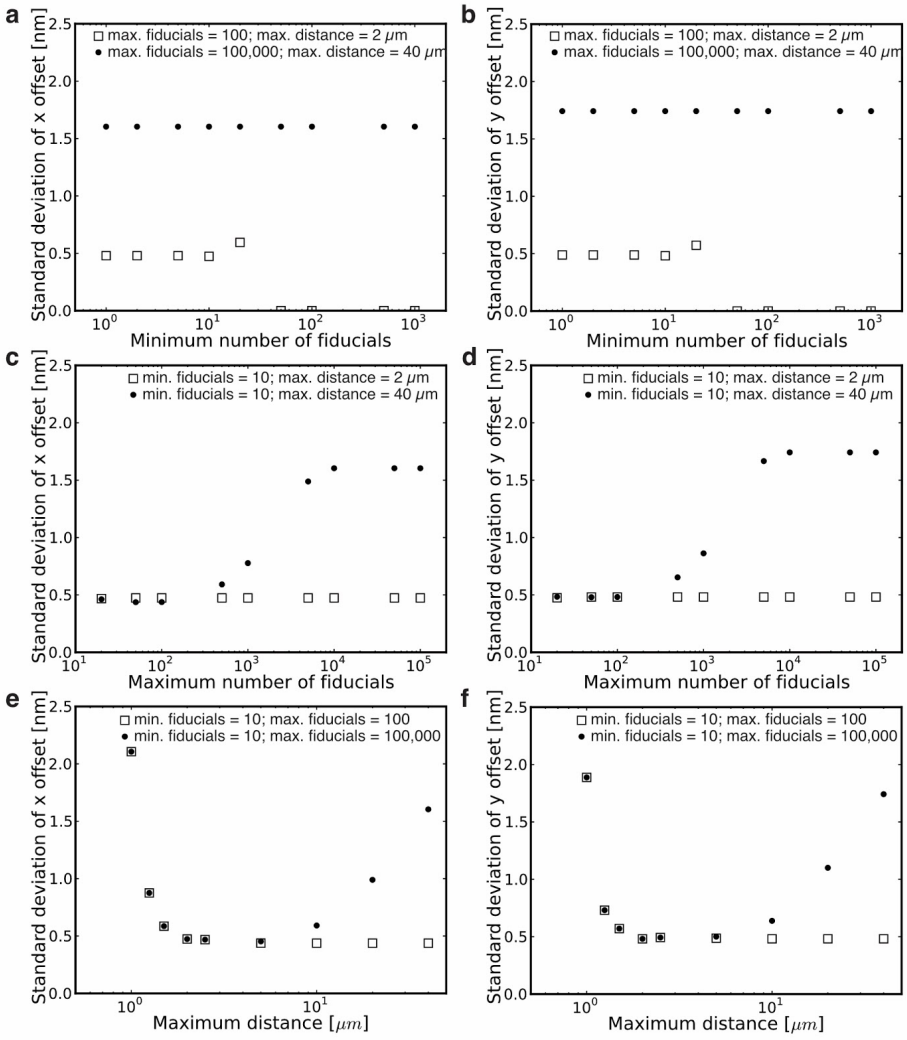

Fig. S4 | Optimization of parameters for piecewise affine image registration. As shown in Fig. S3, different parameter settings for the piecewise affine transformation have a significant effect on the goodness of the registration. Thus, we performed an in-depth analysis of the influence of the following parameter on image registration: minimum and maximum number of fiducial points and maximum distance between points. Also, as shown in Fig. S3 pooling data in 10 μm by 10 μm squares can reveal local biases in registration errors. If the registration error is uncorrelated we expect a random distribution of squares with light shades of red and blue. In such a case, we expect the standard deviation of the squares to be small, whereas a registration with local distortions results in squares with high intensities and hence a larger standard deviation among all squares. Thus, we can use the standard deviation of registration errors of all 10 μm by 10 μm squares as a measure of goodness of registration over the entire field of view. Hence, the lower the standard deviation of the offset, the better the parameter

setting for image registration. (a) Standard deviation of average offset along x-axis of all boxes as a function of minimum number of fiducials. Results are shown for two different settings of maximum number of fiducials and maximum distance (filled circle and empty square). (b) Same as in a but along y-axis. (c) Standard deviation from average offset along x-axis of all boxes as a function of maximum number of fiducials. Results are shown for two different settings of minimum number of fiducials and maximum distance (filled circle and empty square). (d) Same as in c but along y-axis. (e) Standard deviation from average offset along x-axis of all boxes as a function of maximum distance. Results are shown for two different settings of minimum and maximum number of fiducials (filled circle and empty square). (f) Same as in e but along y-axis. Details about fitting parameters in Table S4.

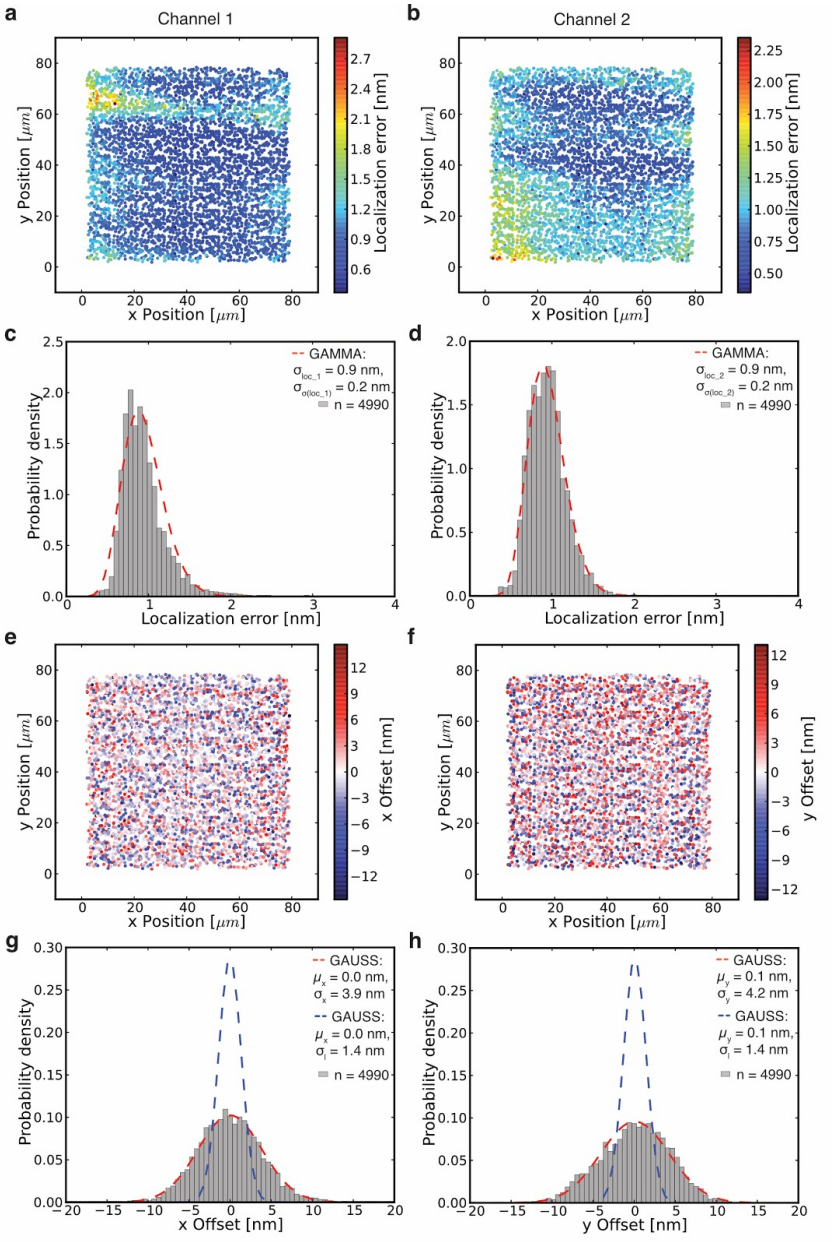

Fig. S5 | Registration precision of TetraSpeck™ beads can not solely be explained by localization errors. If the localization error is the only contributor to the registration imprecision, the uncertainty of localization and registration should be the same. As we see with data, this is not the case for TetraSpeck™ beads because they have not overlapping color centers (Fig. S6). (a) Localization errors in channel 1 of individual TetraSpeck™ beads (each dot represents a single bead) over the entire field of view calculated with maximum likelihood with gaussian (MLEwG) equation from Mortensen et al. (2). Red dots indicate high and blue dots low localization errors. (b) Same as in a but for channel 2. (c) Histogram of localization errors in

channel 1 with fit of gamma distribution (dashed red line) of data shown in a. This clearly shows that the localization errors are different among different beads and that they follow a probability distribution (Fig. S9). (d) Same as in c but for channel 2 and of data in b. (e) Distance offset along the x-axis for same data as shown in a. Negative values (blue dots) mean that channel 1 has a smaller number for its x position whereas positive values (red dots) represent fiducials where channel 2 has a smaller number for its x position. (f) Same as in e but for distance offset along y-axis. (g) Histogram of x-axis offset with Gaussian fit (dashed red line) of data in e. Blue dashed line shows fit if σ_x was only comprised of the localization error σ_l. (h) Same as in g but for offset along y-axis and of data in f. One frame per TetraSpeck™ bead was acquired. Details about fitting parameters in Table S4.

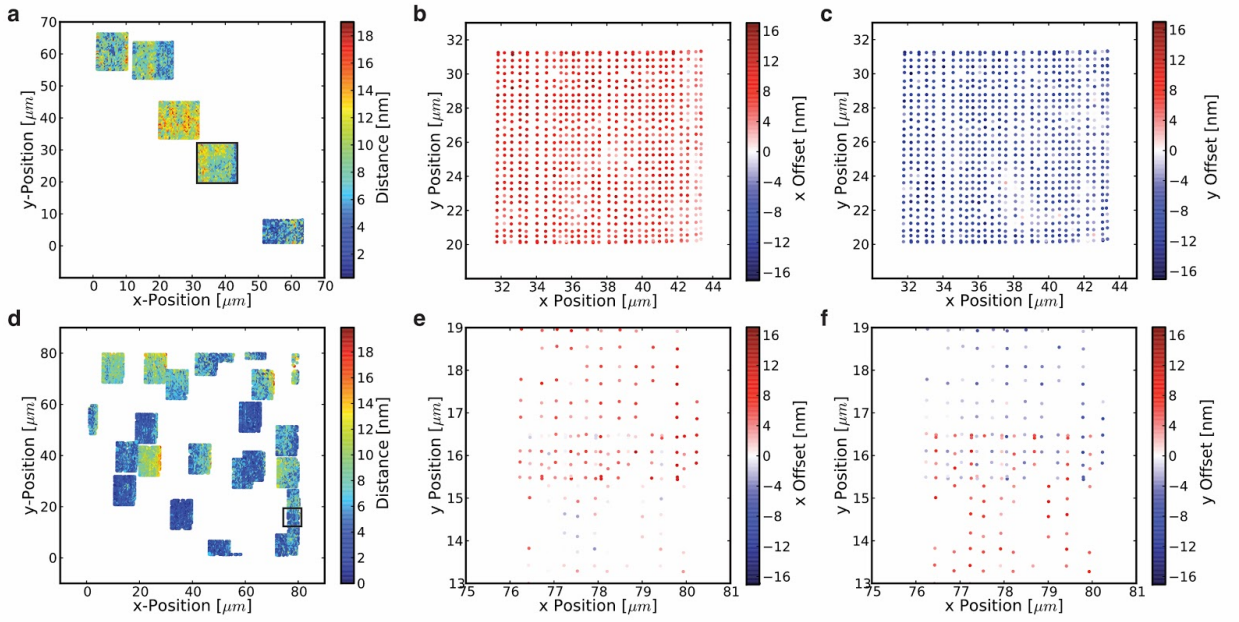

Fig. S6 | TetraSpeck™ beads have an underlying variability and their color centers do not perfectly overlap. (a) Euclidean distance of image registered, 30x30 grid translated, TetraSpeck™ beads. Each grid shows data for one and the same bead. Red dots indicate large and blue dots short distances. Black box highlights area which is shown with higher magnification in b and c. (b) Distance offset along the x-axis of magnified part of micrograph in a. (c) Same as in b but distance offset along y-axis. (d) Euclidean distance of image registered, 20x30 grid translated TetraSpeck™ beads. Each grid shows data for one and the same bead. Red dots indicate large and blue dots short distances. Black box highlights area which is shown with higher magnification in e and f. (e) Distance offset along the x-axis of magnified part of micrograph in d. (f) Same as in e but distance offset along y-axis. Details about fitting parameters in Table S4.

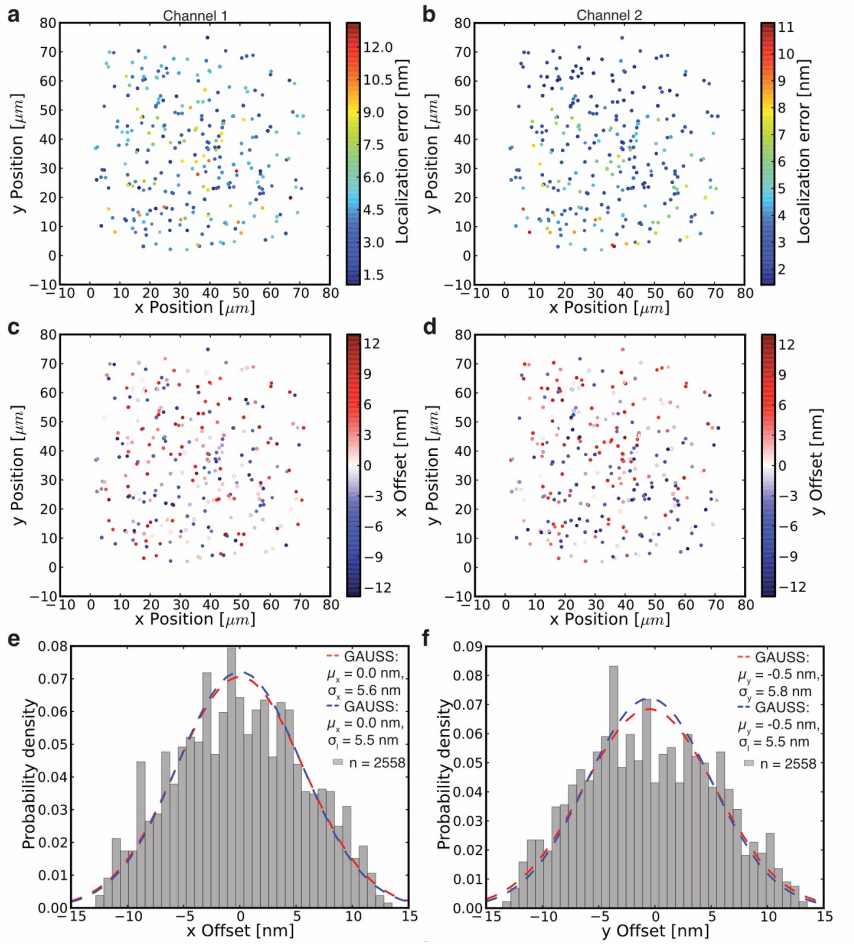

Fig. S7 | Errors in distance measurements are caused by localization errors for a single biotinylated Cy3/Cy5 dsDNA construct. Since the registration imprecision for TetraSpeck™ beads could not fully be explained by localization errors (Fig. S6) but the wider distribution was caused by sample imperfections (non-overlapping color centers), we used a control with perfectly overlapping color centers (3). A 30 bp long double stranded DNA construct was biotinylated and Cy3 labeled on one end, and Cy5 labeled on the other end (3). While attached to the surface at one end through biotin, the other end is free to rotate. Since the tumbling time is much faster than the acquisition time, we expect an average distance between the color centers of zero nanometers. If the localization error is the only contributor to the registration imprecision, the uncertainty of localization and registration should be the same. As we see in these data, this is indeed the case for this construct. (a) Localization errors in channel 1 of Cy3/Cy5 dsDNA construct over the entire field of view calculated with MLEwG equation from Mortensen et al. (2). Red dots indicate high and blue dots low localization errors. (b) Same as in a but for channel 2. (c) Distance offset along the x-axis for same data as shown in a. Negative

values (blue dots) mean that channel 1 has a smaller number for its x position whereas positive values (red dots) represent fiducials where channel 2 has a smaller number for its x position. (d) Same as in c but for distance offset along y-axis. (e) Histogram of x-axis offset with Gaussian fit (dashed red line) of data in c. Blue dashed line shows fit if σ_x was only comprised of the localization error σ_l. (f) Same as in e but for offset along y-axis and of data in d. 20 frames of each molecule were collected. Details about fitting parameters in Table S4.

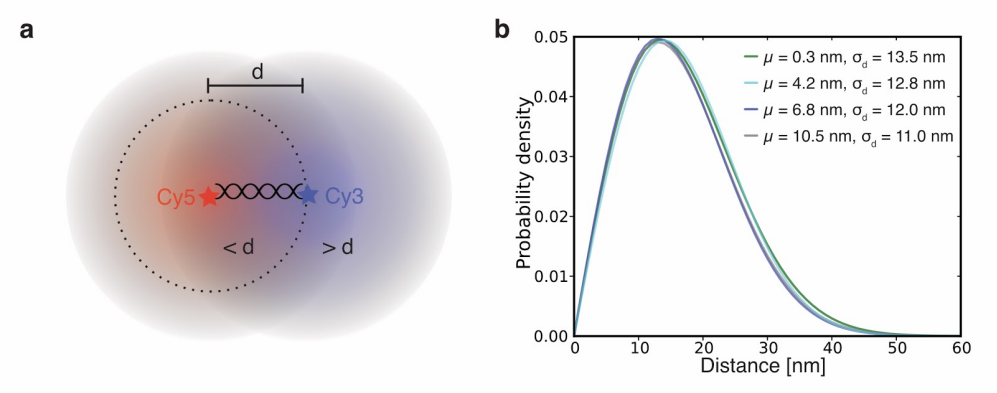

Fig. S8 | Determination of nanometer distances from skewed distributions. (a) Top view of two fluorescence intensity distributions that are separated by distance d. Circle with dotted line has a radius d around the position of the Cy5 molecule. Assuming the true position of Cy5 is known, each measurement that finds Cy3 inside the circle will be less than d and measurements finding Cy3 outside the circle are larger than d. Integrating the intensities of the blue molecule inside and outside the circle shows that the total intensity outside the circle is higher than inside. Consequently, the probability for measuring distances larger than d is higher than measuring distances lower than d. Halos represent position / distance uncertainty. (b) Probability distribution (Eq. 2) plotted for various parameter combinations of calculated distance μ and distance uncertainty σ_d shows that small variations in σ_d lead to large changes in estimation of μ.

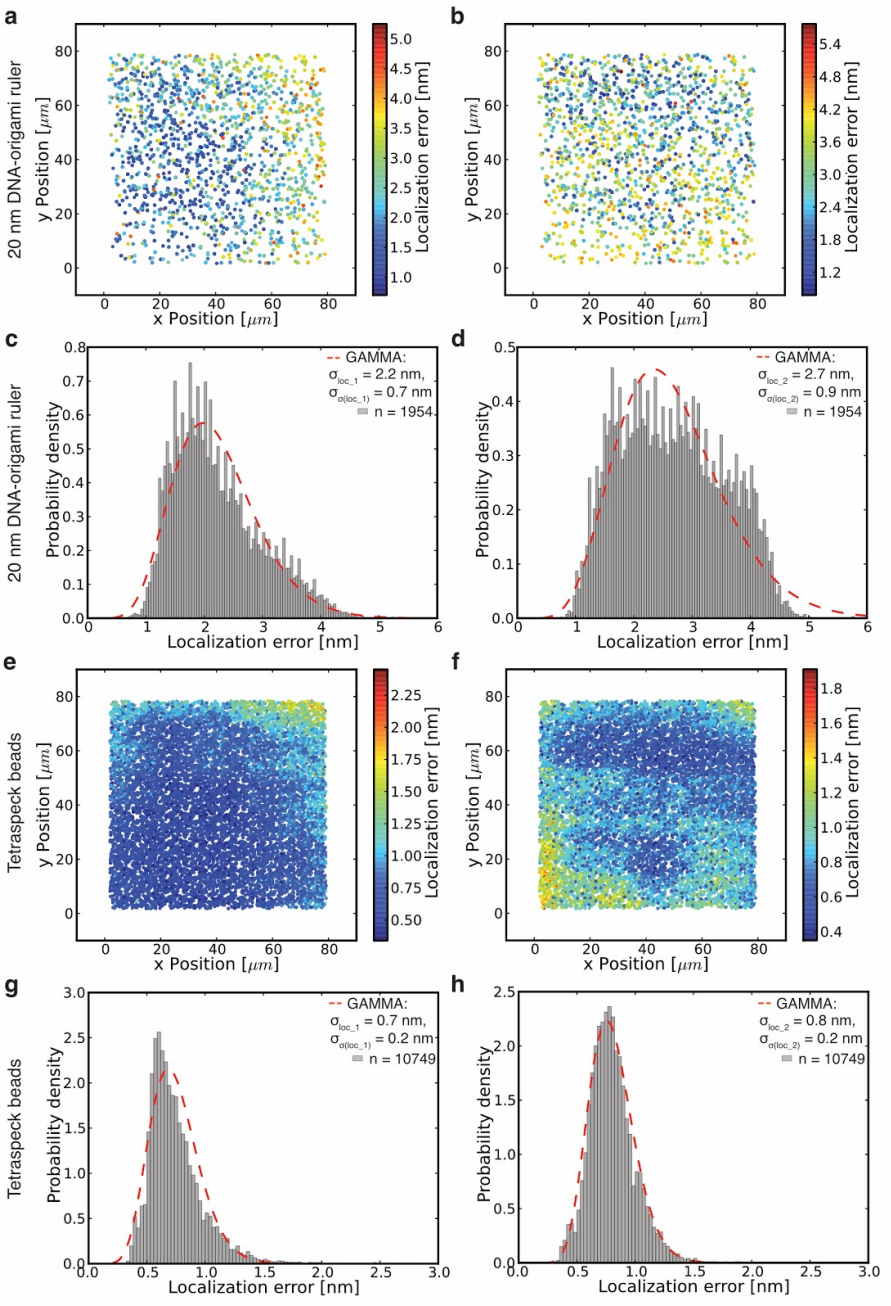

Fig. S9 | Localization errors of many particles have an underlying distribution. Here, we show localization errors over entire field of view for two different probes in two channels. Quantification of 20 nm DNA-origami nanorulers with 5-10 dyes of Cy3 and 5-10 dyes of Alexa 647 whose center of mass is 20 nm apart (a-d), and of TetraSpeck™ beads (e-h). The variation in localization error among different particles is likely caused by the emission of different number of photons, which itself follows a distribution. (a) Localization errors calculated with MLEwG equation from Mortensen et al. (2) in channel 1 (Cy3 or Cy3 like dye(s)) for 20 nm

DNA-origami nanoruler. Red dots indicate high and blue dots low localization errors. (b) Same as in a but for channel 2 (Cy5 or Cy5 like dye(s)). (c) Histogram of localization error in channel 1 for 20 nm DNA-origami nanoruler with fit of gamma distribution (dashed red line) of data shown in a. (d) Same as in c but for channel 2. (e-h) Same as in a-d but for TetraSpeck™ beads. For 20 nm DNA-origami nanoruler 20 frames per molecule were recorded. For TetraSpeck™ beads one frame per molecule was acquired. Details about fitting parameters in Table S4.

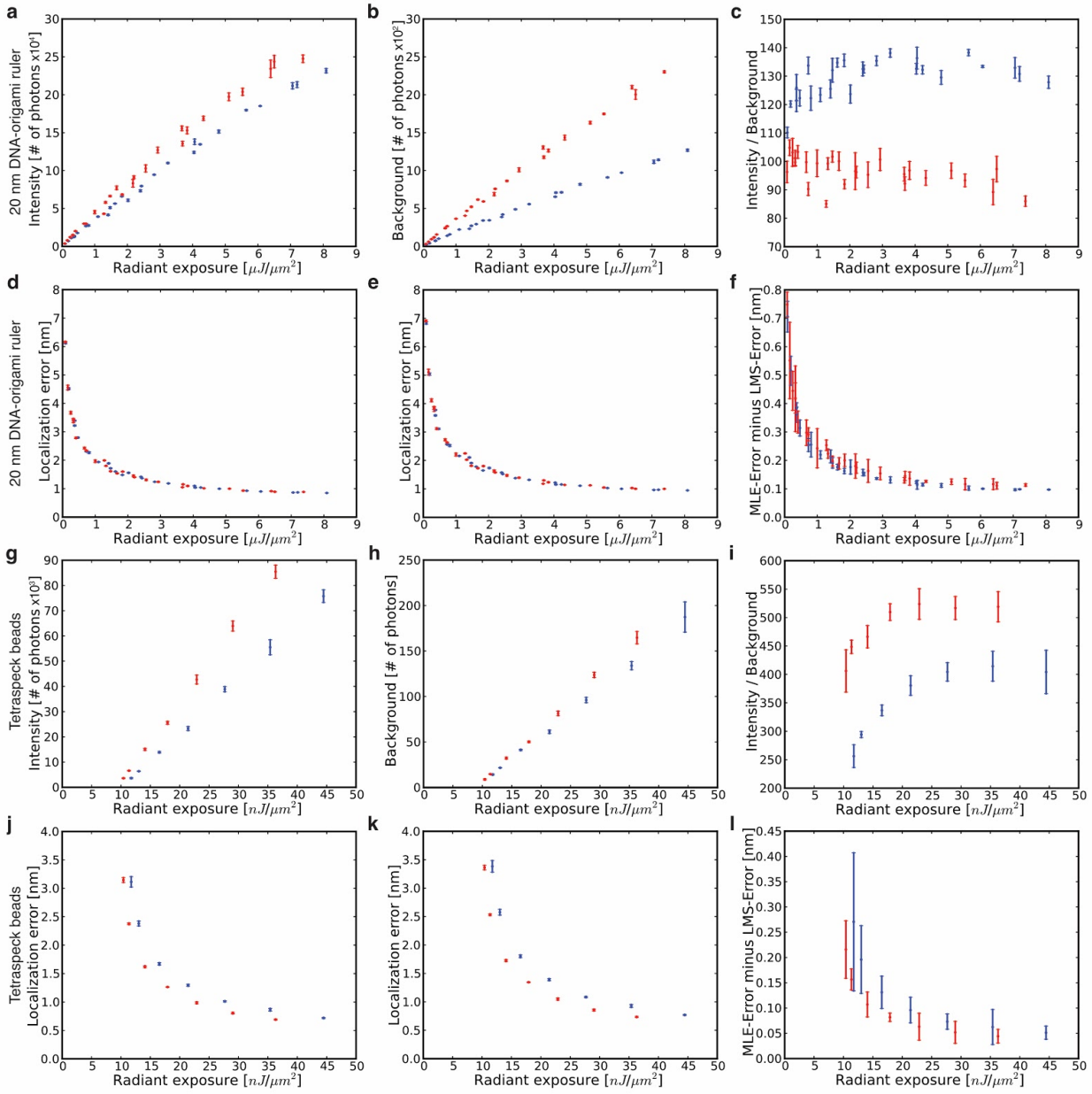

Fig. S10 | Evaluation of photophysical properties of two different probes in two channels. Quantification of 20 nm DNA-origami nanorulers with 5-10 dyes of Cy3 and 5-10 dyes of Alexa 647 whose center of mass is 20 nm apart (a-f), and of TetraSpeck™ beads (g-l). For the intensity as well as the background we expect a linear increase for increasing radiant exposure. Only if for instance photobleaching occurs faster than the acquisition time or if a pixel gets saturated, we expect divergence from the linear behavior. Blue dots show values for channel 1 (Cy3 or Cy3 like dye(s)) and red dots for channel 2 (Cy5 or Cy5 like dye(s)). (a, g) Intensity in number of photons as a function of radiant exposure (Table S2). (b, h) Background in number of

photons as a function of radiant exposure. (c, i) Intensity over background ratio as a function of radiant exposure. (d, j) Localization error calculated with the equation from Thompson et al. (4) (Least Mean Squared (LMS)-Error) as a function of radiant exposure. (e, k) Localization error calculated with the MLEwG equation from Mortensen et al. (2) (MLE-error) as a function of radiant exposure. (f, l) Difference between LMS- and MLE-error as a function of radiant exposure. Error bars in a, b, d, e, g, h, j, and k show standard deviation of five repeats (new microscopy slides with fresh sample). Each repeat consists of at least 100 molecules and one frame was taken per molecule. For c, f, i, and l the error bar is calculated based on error propagation (linear addition). Details about fitting parameters in Table S4.

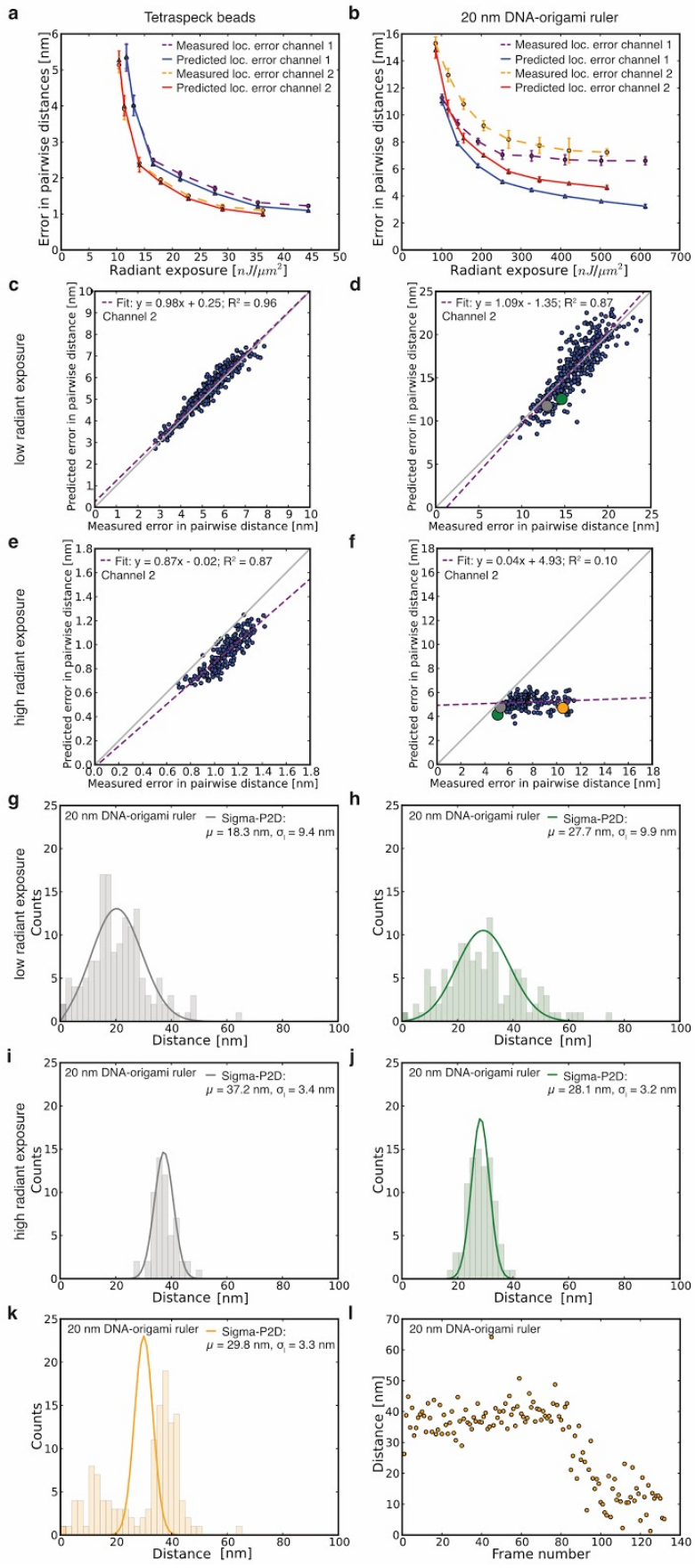
a
Tetraspeck beads
Measured loc. error channel 1
Predicted loc. error channel 1
Measured loc. error channel 2
Predicted loc. error channel 2
Error in pairwise distances [nm]
Radiant exposure [$nJ/\mu m^2$]
b
20 nm DNA-origami ruler
Measured loc. error channel 1
Predicted loc. error channel 1
Measured loc. error channel 2
Predicted loc. error channel 2
Error in pairwise distances [nm]
Radiant exposure [$nJ/\mu m^2$]
c
low radiant exposure
Fit: y = 0.98x + 0.25; R² = 0.96
Channel 2
Predicted error in pairwise distance [nm]
Measured error in pairwise distance [nm]
d
Fit: y = 1.09x - 1.35; R² = 0.87
Channel 2
Predicted error in pairwise distance [nm]
Measured error in pairwise distance [nm]
e
high radiant exposure
Fit: y = 0.87x - 0.02; R² = 0.87
Channel 2
Predicted error in pairwise distance [nm]
Measured error in pairwise distance [nm]
f
Fit: y = 0.04x + 4.93; R² = 0.10
Channel 2
Predicted error in pairwise distance [nm]
Measured error in pairwise distance [nm]
g
low radiant exposure
20 nm DNA-origami ruler
Sigma-P2D:
μ = 18.3 nm, σ_i = 9.4 nm
Counts
Distance [nm]
h
20 nm DNA-origami ruler
Sigma-P2D:
μ = 27.7 nm, σ_i = 9.9 nm
Counts
Distance [nm]
i
high radiant exposure
20 nm DNA-origami ruler
Sigma-P2D:
μ = 37.2 nm, σ_i = 3.4 nm
Counts
Distance [nm]
j
20 nm DNA-origami ruler
Sigma-P2D:
μ = 28.1 nm, σ_i = 3.2 nm
Counts
Distance [nm]
k
20 nm DNA-origami ruler
Sigma-P2D:
μ = 29.8 nm, σ_i = 3.3 nm
Counts
Distance [nm]
l
20 nm DNA-origami ruler
Distance [nm]
Frame number

Fig. S11 | Comparison of measured and predicted localization errors for two different probes in two channels. We evaluated how well measured and predicted localization errors correlate. This is important because Sigma-P2D depends on accurate determination of localization errors and small discrepancies will lead to incorrect distance determination. Quantification of TetraSpeck™ beads (a, c, e), and of 20 nm DNA-origami nanorulers with 5-10 dyes of Cy3 and 5-10 dyes of Alexa 647 whose center of mass is 20 nm apart (b, d, f). (a, b) Predicted errors in pairwise distances calculated with MLEwG equation from Mortensen et al. (2) for channel 1 (Cy3 or Cy3 like dye(s)) in blue and channel 2 (Cy5 or Cy5 like dye(s)) in red as function of radiant exposure (Table S3). Measured error (standard deviation) in pairwise distances for channel 1 in purple and channel 2 in orange as function of radiant exposure (for more details see SI Note 3). (c, d) Scatter plot of predicted over measure error in pairwise distances of individual molecules (blue dots) for lowest radiant exposure in channel 2 from data in a, b. Dashed purple line shows fit of linear regression and gray solid line shows theoretical limit (Cramér–Rao lower bound (5)) for localization errors. (e, f) Same as in c and d but for highest radiant exposure setting. For higher radiant exposures correlations between predicted and measured localization errors were suboptimal. To understand why, we looked at individual molecules for which predicted and measured localization errors correlated poorly, in this case for nanorulers which were imaged at high intensity. For these molecules, we noticed that the distance between colors and therewith either the position of channel 1 or channel 2 changed. Bleaching of individual dyes is likely an important contributor to this position change. The position change leads to an increase in measured localization error since we determined it via pairwise distances (fluctuation in pairwise distance → increase in measured localization error). (d) Larger, colored dots refer to histograms shown in g and h. (f) Larger, colored dots refer to histograms shown in i-k. (g, h) Histogram of distance distribution of a single-molecule of a 20 nm DNA-origami nanoruler at low radiant exposure. Solid line is fit with Sigma-P2D. (i, j, k) Same as g and h but at high radiant exposure. (l) Distance as a function of time (frame number) of a single-molecule of a 20 nm DNA-origami nanoruler (orange dots). Same data as shown in k. Error bars in a and b show standard deviation of three repeats (new microscopy slides with fresh sample). Each repeat consists of at least 120 pairwise distance measurements, the minimum number of frames per molecule was set to 60 and the maximum number of frames to 200. Single-molecule distances in g-l were obtained by selecting time-lapse series of individual molecules (see Table S6). Details about fitting parameters in Table S4.

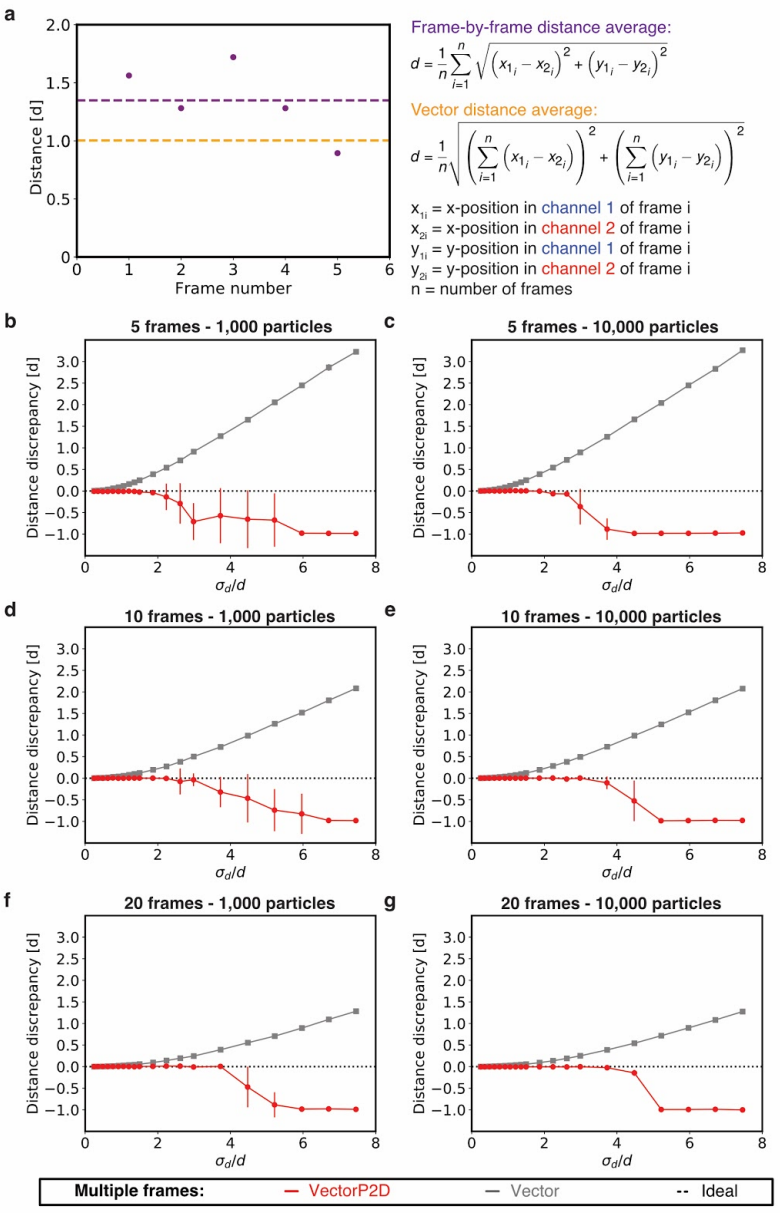

Fig. S12 | Performance of distance prediction by Vector-P2D and Vector methods evaluated with Monte Carlo simulated data. (a) Addition to Fig. 4a: Observed distances for each pair (purple dots) and their average (dashed purple line - d = 1.35) as obtained by a frame-by-frame distance average. To calculate the vector average distance (dashed orange line, resulting in d = 1.0), the average distances in x and y are calculated separately first, before combining them in the overall average distance. (b-g) Additional performance results to those shown in Fig. 4. Here, not 100 particles but 1,000 (b, d, f) and 10,000 (c, e, g) particles were used. Average distance discrepancy for Vector-P2D (red) and Vector (grey) from the true distance was

calculated based on 10 simulations for different ratios of uncertainty σ_d over distance d for 5, 10, and 20 frames. Error bars in b-g show standard deviations of 10 independent simulations.

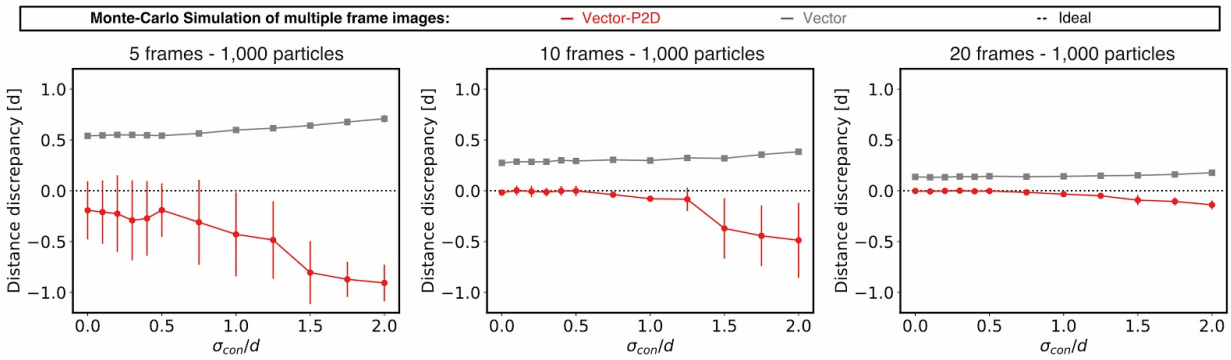

Fig. S13 | Performance of distance prediction as a function of sample heterogeneity of Vector-P2D and Vector using Monte Carlo simulated data. Average discrepancy from the true distance d for Vector-P2D (red) and Vector (grey) was calculated based on 10 simulations for different ratios of sample heterogeneity σ_{con} over distance d for 5, 10, and 20 frames. In all cases we used 1,000 particles and a distance uncertainty σ_d of 2.1. Error bars show standard deviations of 10 independent simulations.

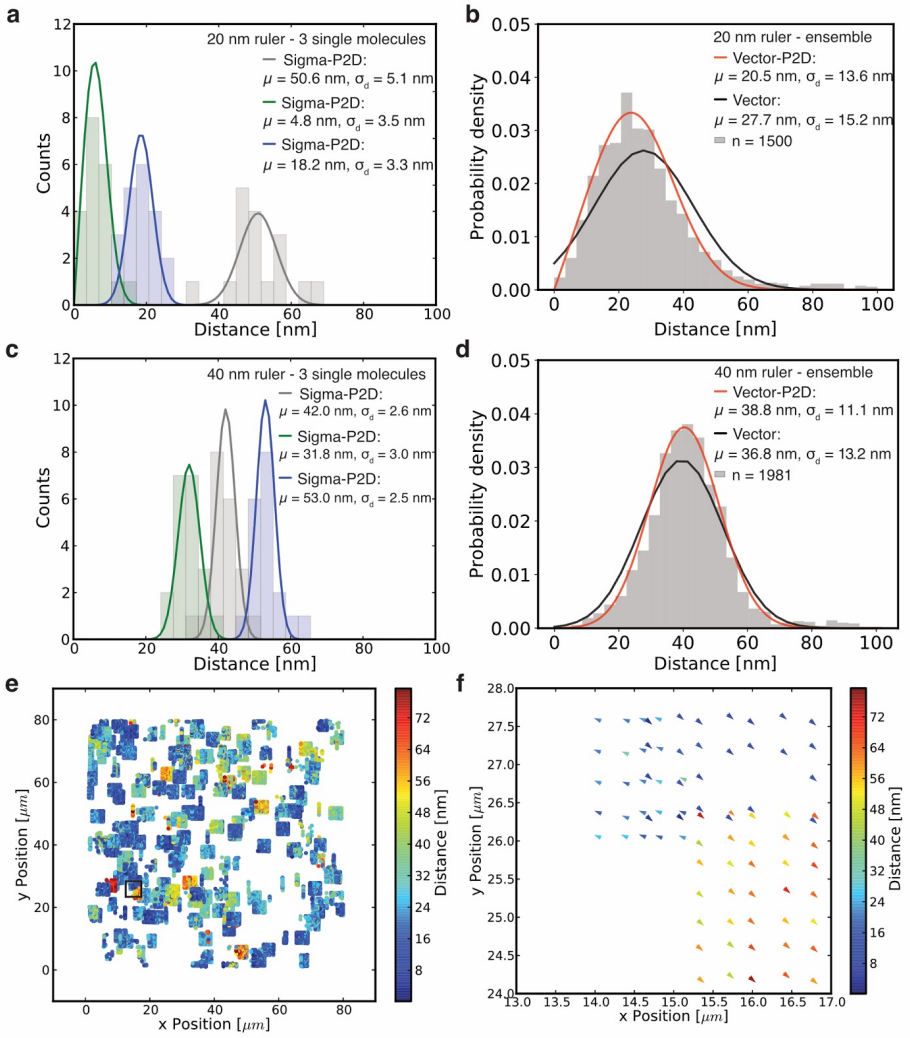

Fig. S14 | Distance measurements for DNA-origami nanorulers. Detailed depiction of results shown in Fig. 4 with distance distributions for single and multiple 20 and 40 nm ruler. (a) Histogram of distance distribution of three different single-molecule 20 nm DNA-origami nanoruler (green, blue, and gray). Solid line is fit with Sigma-P2D. (b) Histogram of vector averaged distance measurements of multiple 20 nm DNA-origami nanorulers analyzed with Vector-P2D (red) and Vector (black). (c) Same as a but for 40 nm DNA-origami nanoruler. (d) Same as b but for 40 nm DNA-origami nanoruler. (e) Euclidean distance of image registered, 12x12 grid translated, 20 nm DNA-origami nanoruler. Each grid shows data for one and the same ruler. Red dots indicate large and blue dots short distances. Black box highlights area shown at higher magnification in f. Some grids of beads will be smaller than 12x12 because of bleaching or dissociation form the microscopy slide. (f) Magnification of highlighted part of micrograph in e. Arrowheads point from position of molecule in channel 1 to its position in

channel 2. Red arrowheads indicate large and blue arrowheads short distances. 20 frames for each molecule in a-d were collected. One frame per molecule was recorded for the grid translated nanorulers in e, f. Details about fitting parameters in Table S4.

a

apo

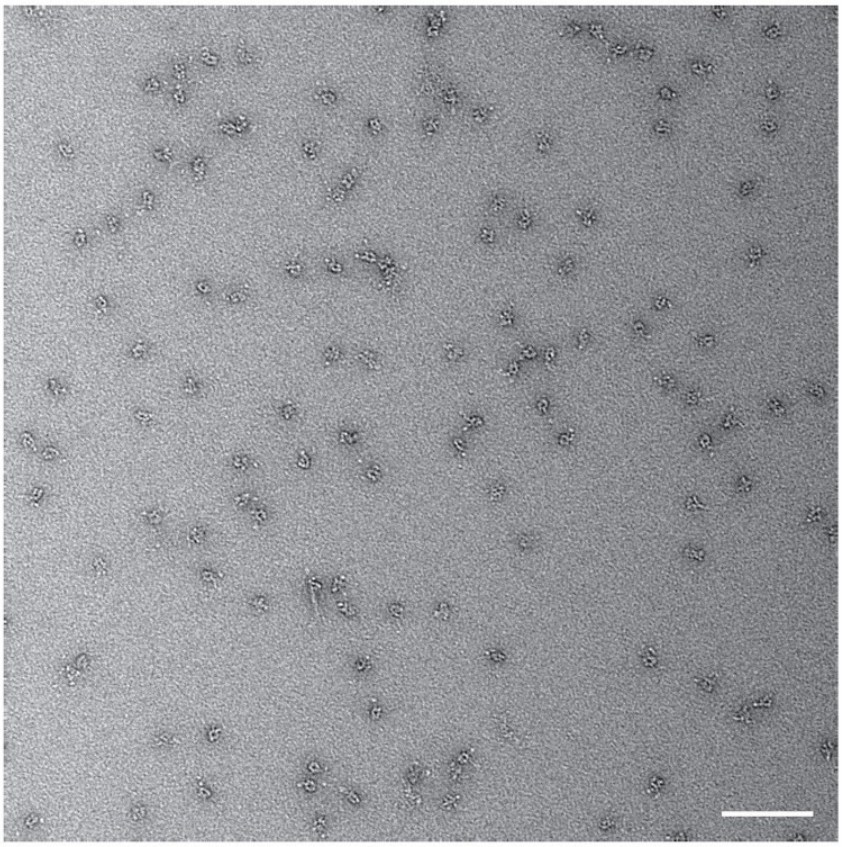

b

ATP-vi

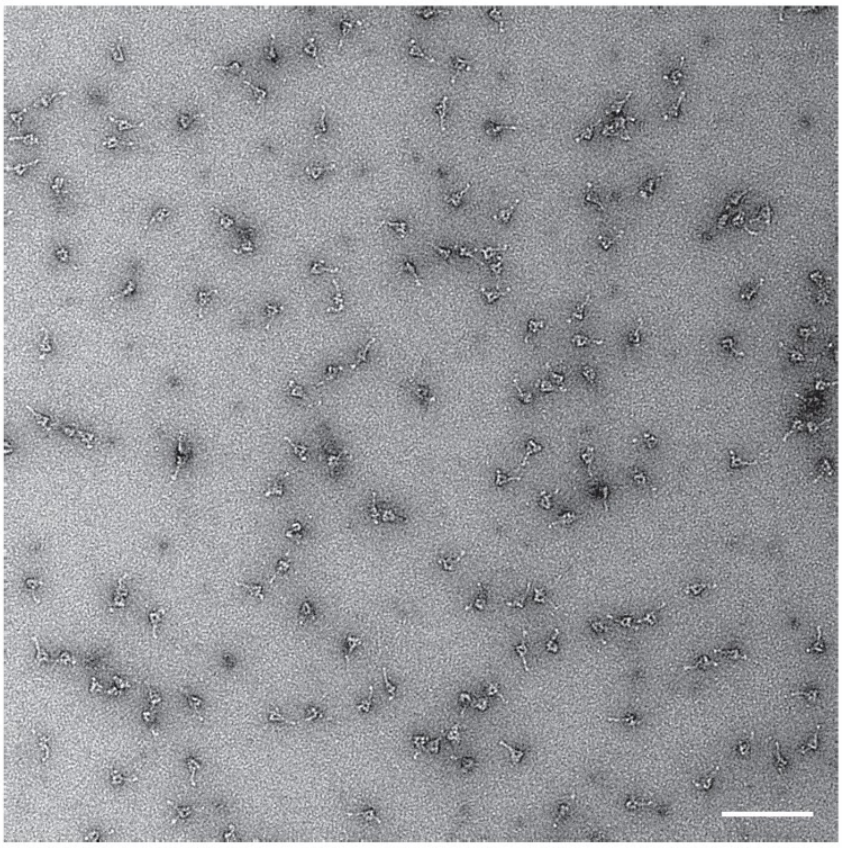

Fig. S15 | Example negative stain electron microscopy micrographs for (a) apo and (b) ATP-vanadate (ATP-vi). For the ATP-vi image, density of the stalk can be seen for many molecules while there is little stalk density for the apo state. Scale bar: 100 nm.

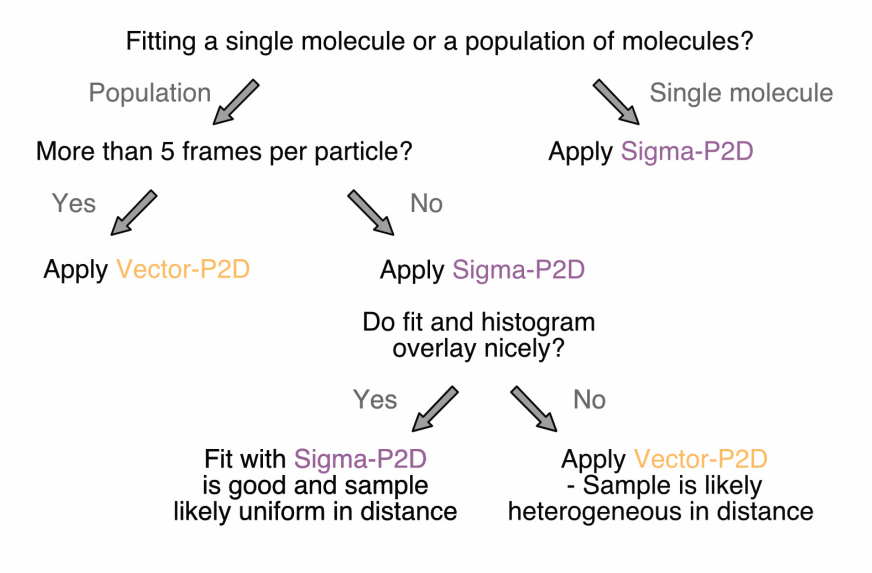

Fig. S16 | Workflow to decide when to use Sigma-P2D or Vector-P2D. This workflow is based on the strength and limitations of each of the two methods as discussed in the discussion section of the manuscript.

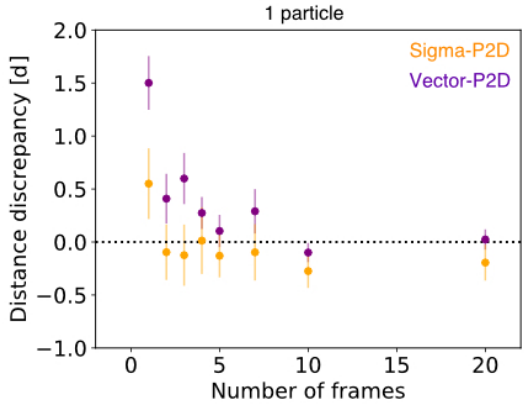

Fig. S17 | Performance of distance prediction as a function of number of frames for Vector-P2D and Sigma-P2D on single particles using Monte Carlo simulated data. Average distance discrepancy for Vector-P2D (purple) and Sigma-P2D (orange) from the true distance was calculated based on 10 simulations for different numbers of frames (observations) of single particles. In all cases we used a distance uncertainty σ_d of 1.5. As can be seen in this data, Sigma-P2D performs better (smaller distance discrepancy) for frames of ~7 and smaller whereas Vector-P2D works better for higher frame numbers of 7 and up. Error bars show standard deviations of 10 independent simulations.

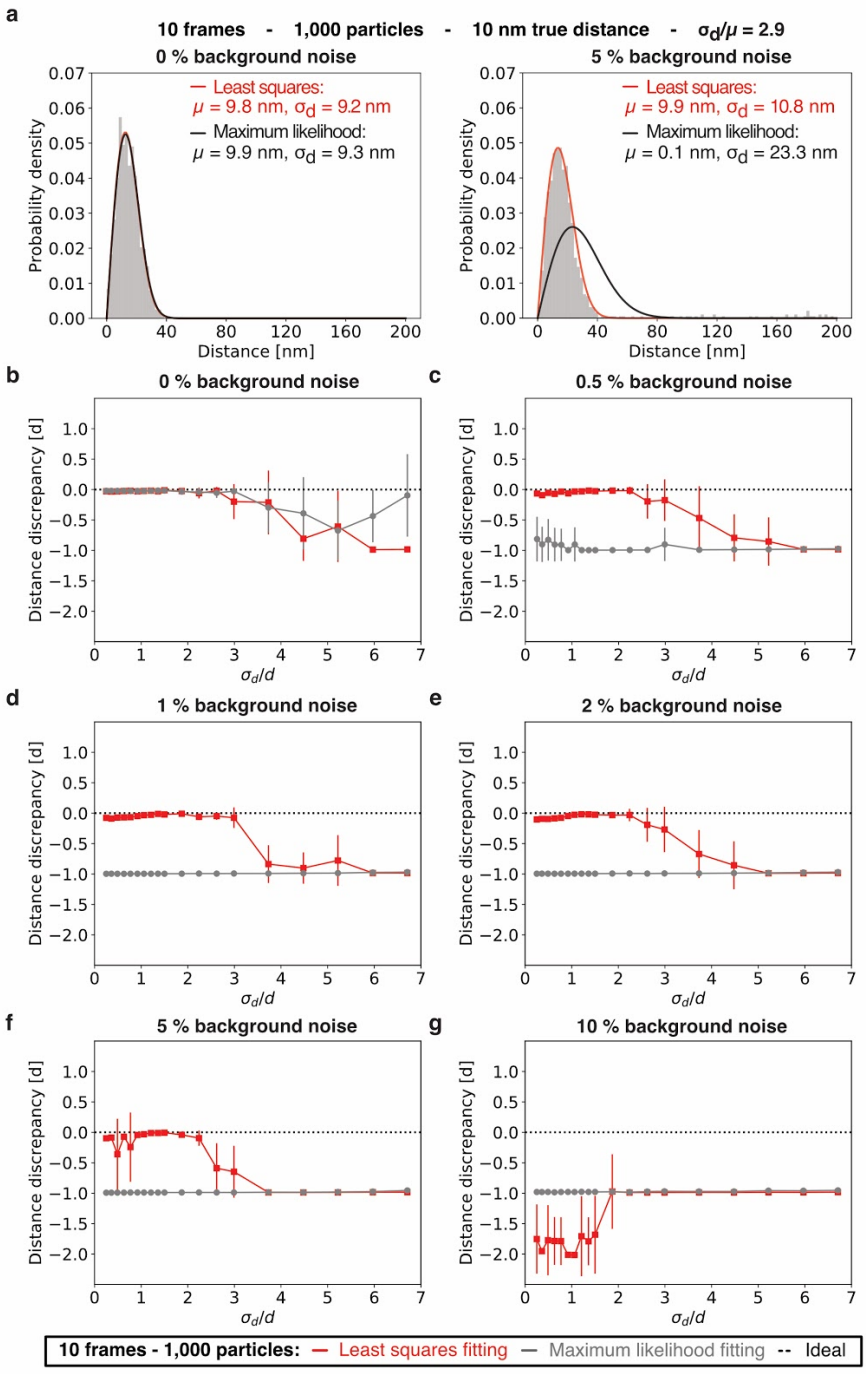

Fig. S18 | Performance of distance prediction by Vector-P2D when fitted by means of maximum likelihood estimation (MLE) or non-linear least squares (NLLSQ) fitting evaluated with Monte Carlo simulated data. (a) Histogram of Monte Carlo simulated data with a true distance d of 10 nm and distance uncertainty σ_d of 29 nm fitted with Vector-P2D by means of MLE (black) and NLLSQ (red). Left: 0% of the data points are background noise. Right: 5 % of all data points are random background noise over a distance from 0 to 200 nm. (b-g) Average

discrepancy from the true distance d for Vector-P2D fitted by means of maximum likelihood estimation (MLE) fitting (grey) or non-linear least squares (NLLSQ) fitting (red) based on 10 simulations for different ratios of sample heterogeneity σ_{con} over distance d and with different amount of background noise (outlier). In all cases we used 1,000 particles and 10 frames. Error bars in b-g show standard deviations of 10 independent simulations.

Supplementary Information Tables

Nucleotide state	full stalk	no stalk	partial stalk	not scored	total
apo	29	1670	157	606	2462
ATP vanadate	2206	104	500	478	3288

Table S1 | Counts of stalk morphology of individual dynein particles in different nucleotide states from negative stain electron microscopy. Number of particles scored as shown in Fig. 5f. Some of the particles could not be assigned to any of the three categories because of ambiguity. Thus, these were assigned to a 'not scored' category and are not taken into account for calculation of the percentages for Fig. 5f. Procedure of scoring is described in Materials and Methods.

Laser power Ch1 [mW]	Laser power Ch2 [mW]	Exposure time [ms]	Radiant exposure Ch1 [nJ/um^2]	Radiant exposure Ch2 [nJ/um^2]	Noise threshold - beads	Noise threshold - 20 nm ruler
0.42	0.38	100	11.75	10.42	100	-
0.47	0.41	100	13.03	11.36	200	-
0.60	0.51	100	16.53	14.08	300	-
0.77	0.65	100	21.42	17.92	400	-
1.00	0.82	100	27.67	22.89	800	-
1.27	1.05	100	35.39	29.03	1,500	-
1.60	1.31	100	44.47	36.31	2,500	-
0.84	0.74	400	93.33	82.22	-	220
0.84	0.74	800	186.67	164.44	-	400
0.84	0.74	1,200	280.00	246.67	-	650
0.84	0.74	1,600	373.33	328.89	-	800
0.84	0.74	2,000	466.67	411.11	-	1,100
3.3	3.0	400	366.7	333.3	-	750
3.3	3.0	800	733.3	666.7	-	1,600
3.3	3.0	1,200	1,100.0	1,000.0	-	2,250
3.3	3.0	1,600	1,466.7	1,333.3	-	2,850
3.3	3.0	2,000	1,833.3	1,666.7	-	3,750
7.3	6.6	400	811.1	733.3	-	1,650
7.3	6.6	800	1,622.2	1,466.7	-	3,300
7.3	6.6	1,200	2,433.3	2,200.0	-	4,500
7.3	6.6	1,600	3,244.4	2,933.3	-	6,000
7.3	6.6	2,000	4,055.6	3,666.7	-	8,000
12.7	11.5	400	1,411.1	1,277.8	-	2,100
12.7	11.5	800	2,822.2	2,555.6	-	5,500

Laser power Ch1 [mW]	Laser power Ch2 [mW]	Exposure time [ms]	Radiant exposure Ch1 [nJ/um^2]	Radiant exposure Ch2 [nJ/um^2]	Noise threshold - beads	Noise threshold - 20 nm ruler
12.7	11.5	1,200	4,233.3	3,833.3	-	8,000
12.7	11.5	1,600	5,644.4	5,111.1	-	10,000
12.7	11.5	2,000	7,055.6	6,388.9	-	12,000
18.2	16.6	400	2,022.2	1,844.4	-	3,500
18.2	16.6	800	4,044.4	3,688.9	-	7,000
18.2	16.6	1,200	6,066.7	5,533.3	-	11,000
18.2	16.6	1,600	8,088.9	7,377.8	-	13,000
18.2	16.6	2,000	10,111.1	9,222.2	-	-
21.6	19.5	400	2,400.0	2,166.7	-	4,300
21.6	19.5	800	4,800.0	4,333.3	-	8,800
21.6	19.5	1,200	7,200.0	6,500.0	-	12,500
21.6	19.5	1,600	9,600.0	8,666.7	-	-
21.6	19.5	2,000	12,000.0	10,833.3	-	-

Table S2 | Calculation of radiant exposures as used in Fig. S10. Laser power was measured after the objective. The field of illumination has a 2D Gaussian shape (reflecting the Gaussian shape of the laser beam), causing the radiant exposure to vary over the field of view. Here, we calculated an average radiant exposure by assuming of field of illumination of 60 µm by 60 µm. Noise threshold refers to settings in µManager's (1) 'Localization Microscopy' plug-in. It was chosen so that approximately the same number molecules was fitted per micrograph and to avoid fitting background as true particles (especially for higher radiant exposures). More details about fitting parameters in Table S4.

Laser power Ch1 [mW]	Laser power Ch2 [mW]	Exposure time [ms]	Radiant exposure Ch1 [nJ/um^2]	Radiant exposure Ch2 [nJ/um^2]	Noise threshold - beads	Noise threshold - 20 nm ruler
0.42	0.38	100	11.75	10.42	100	-
0.47	0.41	100	13.03	11.36	200	-
0.60	0.51	100	16.53	14.08	300	-
0.77	0.65	100	21.42	17.92	400	-
1.00	0.82	100	27.67	22.89	800	-
1.27	1.05	100	35.39	29.03	1,500	-
1.60	1.31	100	44.47	36.31	2,500	-
0.91	0.77	400	101.33	85.11	-	50
1.27	1.05	400	141.00	116.78	-	80
1.73	1.40	400	192.00	155.78	-	95
2.28	1.86	400	253.33	206.11	-	135
2.94	2.42	400	326.78	269.11	-	175
3.7	3.1	400	411.1	346.7	-	230
4.5	3.8	400	502.2	421.1	-	270
5.5	4.7	400	613.3	516.7	-	350

Table S3 | Calculation of radiant exposures as used in Fig. S11. Laser power was measured at objective. The field of illumination has a 2D Gaussian shape (reflecting the Gaussian shape of the laser beam), causing the radiant exposure to vary over the field of view. Here, we calculated an average radiant exposure by assuming of field of illumination of 60 µm by 60 µm. Noise threshold refers to settings in µManager's (1) 'Localization Microscopy' plug-in. It was chosen so that approximately the same number molecules was fitted per micrograph and to avoid fitting background as true particles (especially for higher radiant exposures). More details about fitting parameters in Table S4.

Imaging Parameters	
Photon conversion factor	1.84
Linear (EM) gain	1.0
Pixel size [nm]	159.0
Time interval [ms]	0.0
Z-step [nm]	50.0
Camera offset [electron counts]	91.0
Read noise [electron counts]	9.84
Find Maxima	
Pre-Filter	None
Noise tolerance	See **Table S5**
Fit Parameters	
Dimensions	1
Filter	Simplex-MLE
Max Iterations	500
Box size [pixel]	12.0
Fix width	Not selected
Filter Data	Nothing selected
Positions	Always all, except for registration maps where data is split to create affine and piecewise affine maps so that ~1000 beads can be used for affine map. Remainder is used for piecewise affine map.
Skip Channels	Not selected

Table S4 | Fitting parameters used in μManager's (1) 'Localization Microscopy' plug-in.

Data set in Figure	**Radiant exposure used for sample of interest [nJ/um²]**		**Noise threshold used for sample of interest**
	Channel 1	**Channel 2**	
Fiducials to create *all maps*	35.39	29.03	300
Figure 2	35.39	29.03	300
Figure 3	613.3	516.7	100
Figure 4	613.3	516.7	100
Figure 5	1,982.0	1,853.3	100
Supplementary Figure 2	35.39	29.03	300
Supplementary Figure 3	35.39	29.03	300
Supplementary Figure 4	35.39	29.03	300
Supplementary Figure 5	35.39	29.03	300
Supplementary Figure 6	35.39	29.03	300
Supplementary Figure 7	2,400.0	2,166.7	300
Supplementary Figure 9	20 nm ruler: 613.3 Beads: 35.39	20 nm ruler: 516.7 Beads: 29.03	All data sets: 300
Supplementary Figure 10	See **Table S2**		See **Table S2**
Supplementary Figure 11	See **Table S3**		See **Table S3**
Supplementary Figure 14	a-d: 613.3 e, f: 35.39	a-d: 516.7 e, f: 29.03	a-d: 100 e, f: 300

Table S5 | Radiant exposures used for the acquisition of different data sets if not specified elsewhere. Noise tolerance as used in the µManager's (1) 'Localization Microscopy' plug-in for different data sets if not specified elsewhere.

Data set in Figure	Minimum # of Frames	Maximum # of missing Frames	Maximum Distance [nm]	Minimum total distance [nm]	Combine tracks from all channels	Maximum pair distance [nm]
Figure 3	e, f: 5	e, f: 15	e, f: 15	e, f: 0	e, f: Checked	e, f: 30
Figure 5	c, d: 15	c, d: 5	c, d: 25	c, d: 0	c, d: Checked	c, d: 100
Supplementary Figure 5	a-f: 3 g-l: 3	a-f: 17 g-l: 17	a-f: 20 g-l: 10	a-f: 0 g-l: 0	a-f: Checked g-l: Checked	a-f: 20 g-l: 20
Supplementary Figure 11	60	10	90	0	Unchecked	-

Table S6 | Settings for the 'Extract Tracks' function in the μManager's (1) 'Localization Microscopy' plug-in used to extract tracks of single-molecules that were imaged for F number of frames. Here the maximum distance refers to the distance between the position of one molecule from channel n-1 to channel n. The minimum total distance indicates the distance of one molecules' position in frame 1 to its position in frame F. Maximum pair distance selects molecules in which the distance between channel 1 and channel 2 position is below a defined threshold.

Supplementary Information Note 1

Color centers of TetraSpeck™ beads do not overlap

For TetraSpeck™ beads the registration precision (σ_x, σ_y) is worse than one would expect based on their localization errors σ_l (σ_{loc_1}, σ_{loc_2} and their variances $\sigma_{\sigma(loc\_1)}$, $\sigma_{\sigma(loc\_2)}$) (Fig. S5). To assess if this discrepancy is due to our image registration procedure or an intrinsic parameter of the beads, we imaged individual beads translated in a 30x30 grid pattern and noticed that most beads have a consistent x-y-distance offset, independent of the position in the image (Fig. S6a-c). In an area where grids of two beads overlap we observed that the offset in x and y was a function of the individual bead, not the position in the image (Fig. S6d-f). As reported by others (3, 6), this strongly suggests that the offset is caused by beads for which the color centers of the two dyes do not exactly overlap but differ by a few nanometers. To test if the registration precision can solely be explained by localization errors σ_l of the test sample we turned to a single biotinylated Cy3/Cy5 dsDNA construct, which has been shown to have no distance variation across molecules and to be of zero distance (3). Using both low and high radiant exposures, we found very good agreement between μ_x and σ_l as well as μ_y and σ_l (Fig. S7). Thus, these experiments suggest that the sample's localization error σ_l can almost solely account for the registration precision σ_{reg} as long as the sample is uniform in distance and the registration accuracy is high (< 1 nm).

Supplementary Information Note 2

The two-dimensional probability distribution (7) is given by

$$p_{2D}(r) = \left(\frac{r}{\sigma_d^2}\right) exp\left(-\frac{\mu^2+r^2}{2\sigma_d^2}\right) I_0\left(\frac{r\mu}{\sigma_d^2}\right) \tag{4}$$

in which r is the measured Euclidean distance, μ the calculated distance, σ_d the distance uncertainty, and I_0 the modified Bessel function of integer order zero. For $\sigma_d \gg \mu$, r similar order or less than σ_d, and with

$$I_0(z) = \sum_{k=0}^{\infty} \frac{\left(\frac{1}{4}z^2\right)^k}{(k!)^2} \tag{5}$$

we can find the following approximation:

$$p_{2D}(r) \approx \left(\frac{r}{\sigma_d^2}\right) exp\left(-\frac{\mu^2+r^2}{2\sigma_d^2}\right)\left(1 + \frac{r^2\mu^2}{4\sigma_d^4} + ...\right) \tag{6}$$

$$\approx \left(\frac{r}{\sigma_d^2}\right) exp\left(-\frac{r^2}{2\sigma_d^2}\right)\left(1 - \frac{\mu^2}{2\sigma_d^2} + ...\right)\left(1 + \frac{r^2\mu^2}{4\sigma_d^4}\right) \tag{7}$$

$$\approx \left(\frac{r}{\sigma_d^2}\right) exp\left(-\frac{r^2}{2\sigma_d^2}\right)\left(1 + \frac{\mu^2}{2\sigma_d^2}\left(\frac{r^2}{2\sigma_d^2} - 1\right)\right) \tag{8}$$

$$\approx \left(\frac{r}{\sigma_d^2}\right) exp\left(-\frac{r^2}{2\sigma_d^2}\right) \tag{9}$$

Thus, the approximation for $\sigma_d \gg \mu$ of the probability distribution (Eq. 2 / 4) is independent of μ.

Supplementary Information Note 3

Predicted and measured localization errors correlate well

Sigma-P2D can only be used with experimental data if the fluorophores' localization errors can be determined with high accuracy, because imprecise predictions lead to incorrect distance estimates (Fig. S8b). To test the available theoretical predictions of localization errors, we first imaged fluorescent probes that varied in number of fluorophores and determined intensities, backgrounds and widths using the MLE Gaussian fit (2). Based on these measurements, we compared the localization errors given by the equations of Thompson et al. (4) and the MLEwG method described by Mortensen et al. (2) (Fig. S10). Both equations yielded fairly similar values, with the MLEwG resulting in slightly higher localization errors, as reported previously (2, 8).

We then investigated the standard deviation of localization errors ($\sigma_{\sigma(loc\_1)}$, $\sigma_{\sigma(loc\_2)}$) for fluorescent probes with a cluster of up to ten Cy3 and Alexa 647 dyes (20 nm nanorulers), and of TetraSpeck™ beads. We found that localization errors follow a probability distribution (Fig. S9) that depends amongst other things on the illumination pattern and the number of fluorophores per particle. Thus, in order to plot a fit for Sigma-P2D of many molecules the distance uncertainty $\sigma_{d\text{-}adj}$ has to be adjusted to

$$\sigma_{d-adj} = \sqrt{\sigma_{reg}{}^2 + \sigma_{loc_1}{}^2 + \sigma_{loc_2}{}^2 + \sigma_{\sigma_{loc_1}}{}^2 + \sigma_{\sigma_{loc_2}}{}^2}\,. \tag{10}$$

Note, that the distance μ is still determined as described above by performing MLE for individual particles using equations 2 and 3 and we only need this adjusted distance uncertainty $\sigma_{d\text{-}adj}$ if we plot a fit for a histogram with distances of many particles.

Next, we measured localization errors at various radiant exposures and compared these to those predicted by equations. We measured the variations in probe position in a time-lapse sequence to determine the experimental localization error. We determined the localization error of each probe by averaging the variance of its pairwise distance with each of the other probes in the image over more than 120 frames (see Materials and Methods). The error predicted by the MLEwG fit for a single probe was calculated from the average pairwise localization error of that probe with all other probes from the same dataset. Interestingly, the measured and

predicted localization errors correlate well ($R^2 \geq 0.8$) at low radiant exposures (Fig. S11) but poorly for one of the two samples at high radiant exposures (Fig. S11f). We discovered that the poor correlation was caused by intersample distance changes during the measurements likely caused by photobleaching (Fig. S11). To test this further we performed Sigma-P2D on single-molecules from the same dataset (Fig. S11g-l) and noticed that the discrepancy between measured and predicted localization errors for samples with few fluorophores at high radiant exposures is mainly due to intersample distance changes (bleaching of dyes and change in 'center-of-mass' - distance between the two colors) during measurements (Fig. S11k, l). Hence, outliers for which the predicted and measured localization errors do not match are likely caused by sample imperfections. Taken together, the localization errors predicted by the MLEwG method described by Mortensen et al. (2) match the experimentally measured values well.

Supplementary Information Protocol

In the following sections we provide a detailed protocol for data acquisition, fitting of emitters, image registration, and data analysis (distance determination) in µManager (1) 2.0. In addition, we provide screenshots of the relevant plugins.

a) Data acquisition

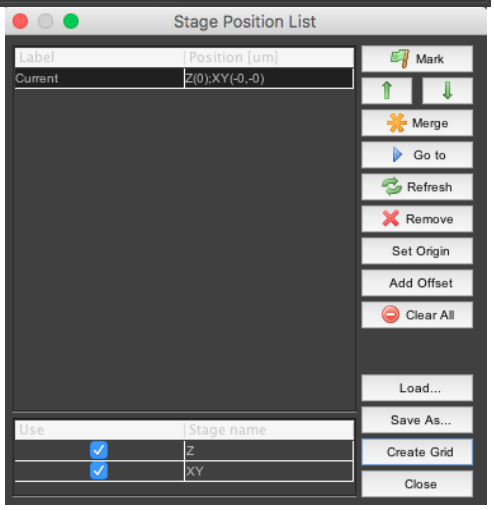

1. Data is acquired in the order depicted in Fig. 2a and as described in the Materials and Methods. For all data collections we used the ‘Multi-Dimensional Acquisition’ plugin. A detailed manual for data acquisition can be found here. Here we only describe the grid acquisition used for fiducial markers.
2. For the fiducial markers to be used for the affine and piecewise affine maps as well as the fiducials used to test the map acquired after the sample of interest, select ‘Multiple Positions’, ‘Channels’ and ‘Save Data’ in the ‘Multi-Dimensional Acquisition’ plugin. Then, click on ‘Edit Position List’. A new window ‘Stage Position List’ will appear.
3. If there are entries in the table, click ‘Clear All’ first. Then click ‘Create Grid’. An additional window ‘Tile Creator’ will open. By clicking ‘+’ and ‘-’ you can increase or decrease the grid size, respectively. Typically you want to create a 20x20 grid. Afterwards type the overlap size and provide the pixel size. We used an overlap of 71 µm for a micrograph of 81x81 µm. Next, click ‘Center Here’ and then ‘OK’.

4. In the ‘Stage Position List’ window all generated positions for your grid will be listed in the table. If everything looks good, click ‘Close’.
5. For how to change ‘Channel’ and ‘Save Data’ settings see here. Once everything is set, click ‘Acquire!’.

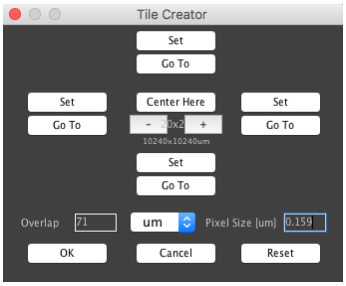

b) Fitting emitters

6. Open the data with the fiducial markers that were acquired **prior** to the sample of interest by either dragging and dropping the file into μManager or by ‘File’ → ‘Open (RAM)’.
7. Open the ‘Localization Microscopy’ plugin: “Plugins’ → ‘Acquisition Tools’ → ‘Localization Microscopy’ that looks like the one on the bottom right of this page.
8. Provide the ‘Imaging parameters’ that match your settings. For the ‘Find Maxima’ you can use the ‘show’ button to see which particles will get selected with the corresponding ‘Noise tolerance’. For the ‘Fit Parameters’ you want ‘Dimensions’ to be ‘1’, and use the ‘Simplex MLE’ ‘Fitter’. We always used ‘500’ as ‘Max Iterations’. The ‘Box Size’ should not be too small because this will overestimate the background. Typically the box size is right when the localization error no longer changes with increasing box size. You can ‘Filter Data’ to remove outliers (optional). If you run any of the example data sets that we provide, use the values listed in Table S4.
9. In ‘Positions’ (Positions of your grid (e.g. you may have acquired a 20x20 grid and thus 400 images total)) start with ‘1-20’ and adjust so that you get approximately 1000 spots to create your affine map. Then click ‘Fit’. A new window ‘Gaussian tracking data’ will open (see below). The number of spots will be listed in the third column.
10. Use the remaining positions (e.g. ‘21-400’) and click ‘Fit’ again. These fiducial markers will be used to create the piecewise affine map.

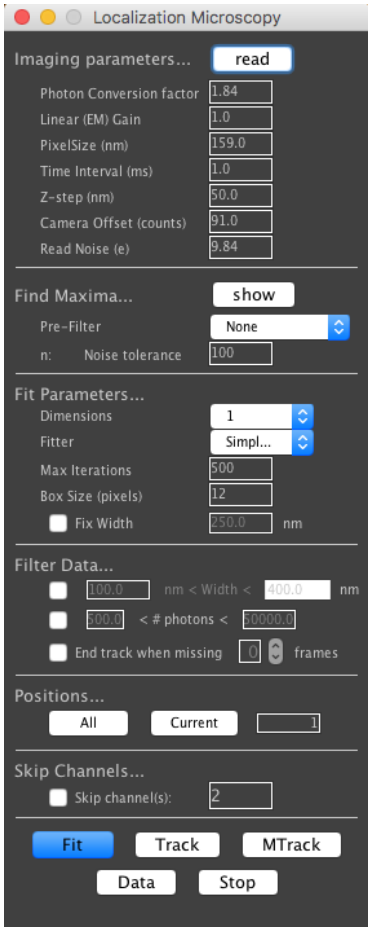

11. Open the data with fiducial markers that were acquired **after** to the sample of interest as described in step 6. This data can be used to test your map (determine the TRE as described in Materials and Methods).
12. Set ‘Positions’ to ‘1-400’ if you acquired a 20x20 grid and click ‘Fit’.
13. Now open a movie/image with the sample of interest as described in step 6. In the ‘Localization Microscopy’ plugin you may want to adjust the ‘Noise Threshold’. Moreover, change ‘Positions’ to ‘1’ since you likely either acquired only a single image or a timelapse movie and did not move to other positions. Then click ‘Fit’.
14. Repeat step 13 for all movies with your sample of interest.

b) Image registration

15. Select the data that you want to use for your affine map (typically the data of fiducials that you fitted in step 9) by clicking on the corresponding row.
16. In ‘2-Color’ select ‘Affine’ from the drop-down menu and use a radius of 2000 nm. Then click ‘2C Reference’.
17. Select all other data including fiducials that will be used as your piecewise affine map, and to test your map as well as all data sets with your sample of interest. Then click ‘Correct’ in ‘2-Color’. This will create new rows with the affine corrected data.
18. Now select the affine corrected version of your data that will be used as the piecewise affine map. Often the maps will have a few fiducials that have a very different two-color distances than most others and might throw off the map. To remove those use ‘Pair Filters’ in the ‘Gaussian tracking data’ window with the following setting: Max dist(nm) = 50 nm, Max sigma = 2, # Quadrants = 36. Then click ‘Filter Now’. This will create a new row with data which is your affine corrected and outlier removed data set to be used as the piecewise affine map.
19. Select the data created in step 18 and chose ‘Piecewise Affine’ from the ‘2-Color’ drop-down menu and a radius of 100 nm (unless you want to measure distances significantly larger than 100 nm, in which case you should set it approximately three fold higher than the expected average distance). Then click ‘2C Reference’.
20. Now you want to set the parameters (Minimum and maximum number of fiducials, Maximum distance) for the piecewise affine map. Since we learnt that ‘10’ is the ideal number as minimum points, this value can not be changed. However, the maximum

number (default ‘100’) and maximum distance (default ‘2000’) can be adjusted. Therefore create a custom script:

```
import edu.ucsf.valelab.gaussianfit.DataCollectionForm;
dcf = DataCollectionForm.getInstance();
dcf.setPieceWiseAffineParameters(100, 2000);
```

Click ‘Run’.

21. Next, select the affine corrected versions of the fiducial data that will be used to test the map and all affine corrected data of your sample of interest. Then click ‘2C Correct’. This command will carry out the piecewise affine transform to correct all your data.
22. At this point you may find it useful to save your data. Select all rows you want to save. Select ‘Text’ and click ‘Save’ in ‘General’ in the ‘Gaussian tracking data’ window. In case you want to load data, you can either click ‘Load’ or drag ‘n drop the ‘.txt’ files into the ‘Gaussian tracking data’ window. The binary format is described in detail here: https://micro-manager.org/wiki/Tagged_Spot_File_(tsf)_format.
23. To determine the registration error, select the piecewise affine corrected version of the fiducial data that will be used to test the map and click ‘List Pairs’ in the ‘Gaussian tracking data’ window and a new window (‘Pair display options’) will open. Then select ‘Show X-Y distance histogram (registration error)’. You may also want to adjust ‘Maximum distance’ to typically 30. Then click ‘OK’. This will open histograms with the registration error in x and y. These can be saved as a ‘.png’ by right click → ‘Save as …’. In addition, a window that shows the final calculated registration error will open and can be saved as a ‘.txt’ by right clicking → ‘Save As...’.
24. In case you want to filter any of your files by number of photons (Intensity) or localization error (Sigma), select the corresponding rows. Then type the desired values in ‘Filters’ in the ‘Gaussian tracking data’ window and click ‘Filter Now’. As before, this will create new data/rows with your filtered data sets.

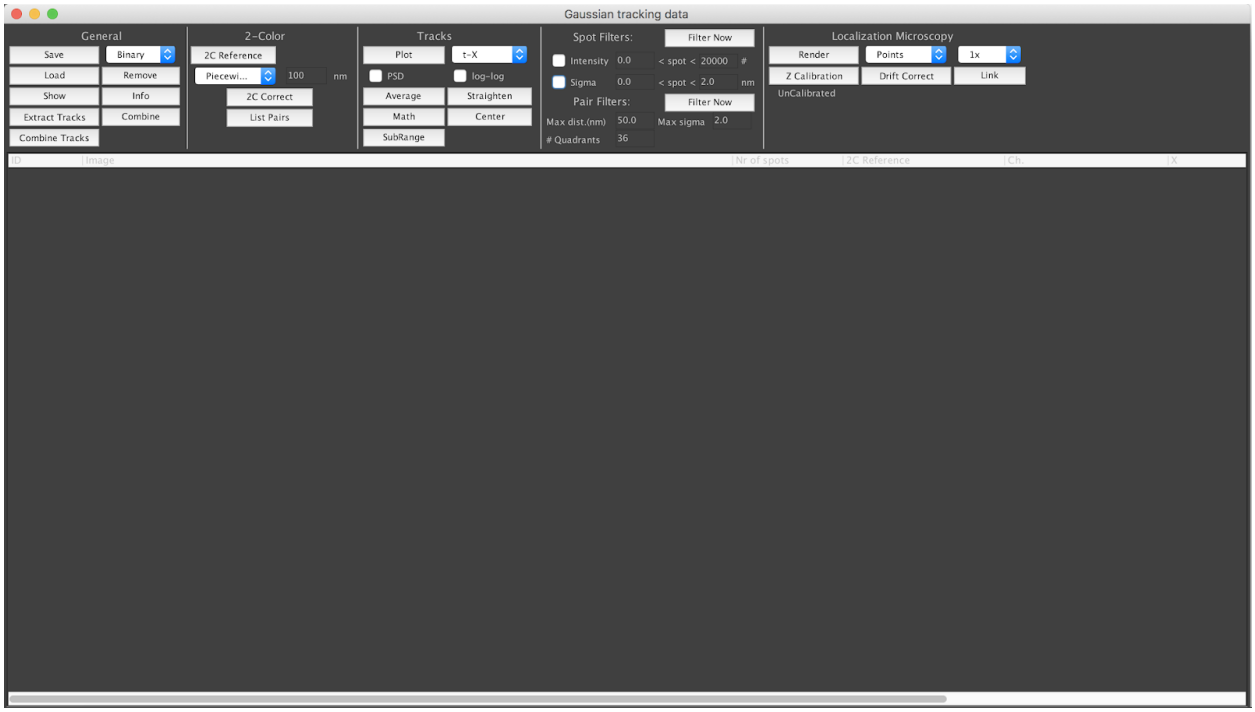

d) Data analysis and distance determination

25. If you have more than one movie/image of your sample of interest, you may want to combine all of them now. Select all desired files/rows and click ‘Combine’ in ‘General’ in the ‘Gaussian tracking data’ window. This will create a data set/row with all files combined. However, when files get combined they still keep unique identifiers. In this case different movies will be assigned different positions. You can see this by selecting the file with the combined data and by clicking ‘Show’. This will open a window with all relevant values like frame number, channel, position, intensity (# of photons), and sigma (localization error). Note, this is the exact same data, that gets saved, when you click ‘Save’.

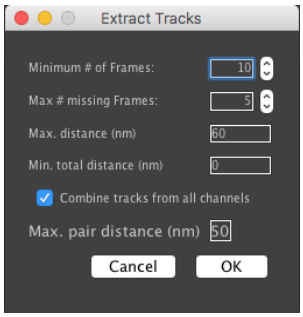

26. This step is optional and only required if you want to extract tracks with defined parameters (remove outliers). A ‘Track’ here refers to the data (localizations) of the same spot that was imaged over multiple times (timelapse). Thus, if you acquired a single image only, you should skip this step.

    Select either individual files of your data of interest or the combined version as created in step 25. Then click ‘Extract Tracks’. This will open a window as shown above. Here is what each of the settings mean:

a. ‘Minimum # of frames’: Say you acquired movies with 20 frames, then you may want to select only spots that have more than 15 frames total to remove spots that bleached earlier or that blinked a lot.
b. ‘Max # of missing Frames’: Define how many frames can be missing (due to blinking) between the first and last localization.
c. ‘Max distance (nm)’: This determines how far localization n can be away from localization n-1 (e.g. it should not jump by 1000 nm).
d. ‘Min total distance (nm)’: Irrelevant here. Set to ‘0’.
e. ‘Combine tracks from channels’: If selected, it will combine tracks from channel 1 and 2 which have localizations in at least one and the same frame that are less than ‘Max. pair distances (nm)’ apart.
f. ‘Max. pair distances (nm)’: See ‘Combine tracks from channels’.

Select your values. If you run any of the example data that we provided, use the values as listed in Table S6. Then click ‘OK’. This will create new rows for each track. Typically you will only care about tracks that have both, channel 1 and 2. These will be listed in the fifth column in the table of the ‘Gaussian tracking data’ window as ‘1,2’. Now, you can combine all tracks that have both channels by selecting these and by clicking ‘Combine’ (similar to step 25).

27. Now, you can determine the distance. Select either data as combined in step 25, or the ‘Extract Tracks’ purified data from step 26, or individual tracks of a single-molecule that you created in step 26. Then click ‘List Pairs’ and a new window (‘Pair display options’) will open. Here you have various options discussed below (all can be executed at the same time):

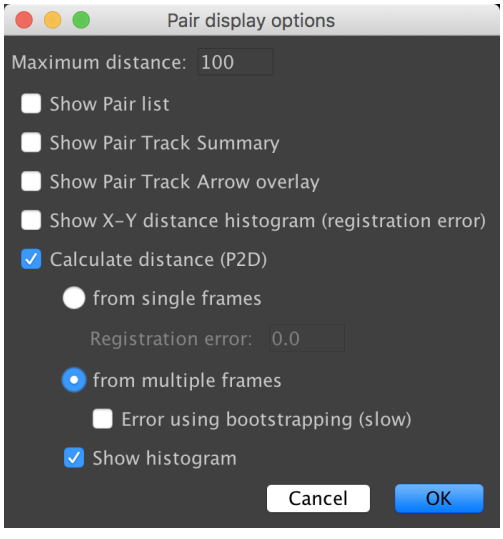

a. ‘Maximum distance’: Provide the cutoff for the maximum distance of a dye pair. This should not be larger than the value you used for the piecewise affine map in step 19.
b. ‘Show Pair list’: If selected, this will open a window with values like all pairwise distances, position, frame number, and localization errors of individual dye pairs. You can save this table by right click → ‘Save As...’.

c. ‘Show Pair Track Summary’: Can only be used if more than one frame per position was acquired (movie but not single image). If selected, this will open a window with values of all frame-by-frame distance averages and their standard deviation, vector distance averages and their standard deviations, number of frames, localization errors, and more. You can save this table by right click → ‘Save As...’.
d. ‘Show Pair Track Arrow Overlay’: Draws arrows into the micrograph to show orientation and magnitude of distance of individual pairwise distances. By orientations we mean an arrow pointing from channel 1 to channel 2. This can be useful to quickly evaluate if the registration map creates and larger, correlated patches when plotting the arrows for the corrected fiducial markers that were acquired after the sample of interest.
e. Show X-Y distance histogram (registration error): see above
f. ‘Calculate distance (P2D)’: This function has multiple subcategories and will calculate distances with the corresponding fit:
    i. ‘From single frames’: executes Sigma-P2D (you can provide the registration error as determined above)
    ii. ‘From multiple frames’: executes Vector-P2D (you can get an error from bootstrapping)
    iii. ‘Show histogram’: Will plot a histogram with the distance distribution and the selected fit(s). This can be saved as a ‘.png’ by right click → ‘Save as …’

Supplementary Information References

1. Edelstein A, Amodaj N, Hoover K, Vale R, Stuurman N (2010) Computer control of microscopes using μManager. *Curr Protoc Mol Biol* Chapter 14:Unit14.20.

2. Mortensen KI, Churchman LS, Spudich JA, Flyvbjerg H (2010) Optimized localization analysis for single-molecule tracking and super-resolution microscopy. *Nat Methods* 7(5):377–381.

3. Pertsinidis A, Zhang Y, Chu S (2010) Subnanometre single-molecule localization, registration and distance measurements. *Nature* 466(7306):647–651.

4. Thompson RE, Larson DR, Webb WW (2002) Precise nanometer localization analysis for individual fluorescent probes. *Biophys J* 82(5):2775–2783.

5. Ober RJ, Ram S, Ward ES (2004) Localization accuracy in single-molecule microscopy. *Biophys J* 86(2):1185–1200.

6. Mortensen KI, Sung J, Flyvbjerg H, Spudich JA (2015) Optimized measurements of separations and angles between intra-molecular fluorescent markers. *Nat Commun* 6:8621.

7. Churchman LS, Flyvbjerg H, Spudich JA (2006) A non-Gaussian distribution quantifies distances measured with fluorescence localization techniques. *Biophys J* 90(2):668–671.

8. Stallinga S, Rieger B (2012) The effect of background on localization uncertainty in single emitter imaging. *2012 9th IEEE International Symposium on Biomedical Imaging (ISBI)*, pp 988–991.